RESEARCH ARTICLE

Interplay between base-salt relief, progradational sediment loading and salt tectonics in the Nordkapp Basin, Barents Sea – Part II

Muhammad Hassaan[1,2] 🄳 | Jan Inge Faleide[1,2] | Roy Helge Gabrielsen[1] |
Filippos Tsikalas[1,3] | Silje Grimstad[4]

[1]Department of Geosciences, University of Oslo, Oslo, Norway

[2]Research Centre for Arctic Petroleum Exploration (ARCEx), University of Tromsø, Tromsø, Norway

[3]Vår Energi AS, Stavanger, Norway

[4]Norges Geotekniske Institutt, Oslo, Norway

Correspondence
Muhammad Hassaan, Department of Geosciences, University of Oslo, P.O. Box 1047 Blindern, NO-0316 Oslo, Norway.
Email: muhammad.hassaan@geo.uio.no

Abstract

Reprocessed, regional, 2D seismic reflection profiles, 3D seismic volumes and well data (exploration and shallow boreholes), combined with 2D structural restorations and 1D backstripping were used to study the post-salt evolution of the Nordkapp Basin in Barents Sea. The post-salt evolution took place above a pre-salt basement and basin configuration affected by multiple rift events that influenced the depositional facies and thickness of Pennsylvanian-lower Permian-layered evaporite sequence. Initially, regional mid-late Permian extension reactivated pre-salt Carboniferous faults, caused minor normal faulting in the Permian strata and triggered slight salt mobilization towards structural highs. The main phase of salt mobilization occurred during earliest Triassic when thick and rapidly prograding sediments entered from the east into the Nordkapp Basin. In the early-mid-Triassic, the change in the direction of progradation and sediment entry-points shifted to the NW led to rotation of the earlier-formed mini-basins and shift of dominant salt evacuation direction to the south. The prograding sediment influx direction, sediment transport velocity and thickness influenced the dynamics of the early to late passive diapirism, salt expulsion and depletion along the strike of the basin. The basin topography resulting from salt highs and mini-basin lows strongly affected the Triassic progradational fairways and determined the distinct sediment routing patterns. Minor rejuvenation of the salt structures and rotation of the mini-basins took place at the Triassic–Jurassic transition, due to far-field stresses caused by the evolving Novaya Zemlya fold-and-thrust belt to the east. This rejuvenation influenced the sediment dispersal routings and caused formation of dwarf secondary mini-basins. The second and main rejuvenation phase took place during likely early-mid-Eocene when propagated far-field stresses from the transpressional Eurekan/Spitsbergen orogeny to the NW inverted pre-salt normal faults, reactivated the structural highs and

rejuvenated the salt structures. The studied processes and study outcomes can be applicable to other evaporite-dominated basins worldwide.

1 | INTRODUCTION

Layered evaporite sequence (LES) of Pennsylvanian to early Permian age is observed in large parts of the Barents Sea and is considered to be deposited under shallow water and arid climate conditions at a paleo-latitude of ca. 30° N (e.g. Larssen et al., 2002; Stemmerik, 2000). The thickest LES is located in tectonically isolated extensional basins, including the Nordkapp, Tiddlybanken and Ottar basins (Figure 1a; Gabrielsen et al., 1990; Hassaan et al., 2021a; Rowan & Lindsø, 2017). The formation of these basins was likely related to the collapse of the Caledonian orogen during the late Devonian and subsequent late Devonian -early Carboniferous NW-SE and late Carboniferous NE-SW oriented regional extension episodes together with regional thermal subsidence conditions (e.g. Gernigon et al., 2018; Rowan & Lindsø, 2017). The Nordkapp Basin is a composite elongated basin with a NW-SE strike that comprises three main segments, that is, the northeastern (NENB), central (CNB) and southwestern (SWNB). The Nordkapp Basin has a prominent dog-leg shape and is ca. 350 km long and ca. 25–87 km wide (Figure 1a). It contains salt pillows, anticlines, walls and stocks that influence the thickness and distribution of the late Permian to Cenozoic strata (Hassaan et al., 2021b; Rojo et al., 2019). Several studies have investigated the growth of salt structures in the Nordkapp Basin during Mesozoic and their impact on the post-salt sedimentary evolution (Grimstad, 2016; Jensen & Sørensen, 1992; Koyi et al., 1993, 1995; Rojo et al., 2019; Rojo & Escalona, 2018; Rowan & Lindsø, 2017). However, these studies were hampered by the low seismic resolution at depth of the available data sets and have overlooked elements related to the LES distribution and pre-salt evolution.

In the current study, we use several vintage and reprocessed 2D regional seismic reflection profiles, 3D seismic data, a new pseudo-3D seismic data cube and available wells (exploration and shallow stratigraphic boreholes; Figure 1b). The aim is to comprehend the interplay between the considerable sediment progradation arriving from the east mainly during the Triassic, the laterally varying LES, and the pre-salt rift architecture in the Nordkapp Basin. Through structural and stratigraphic analyses, 2D kinematic structural restoration and 1D backstripping, we

Highlights

- Interplay between pre-salt rift architecture, layered evaporite sequence and prograding sediments.
- Dependence of salt expulsion and depletion on sediment progradation direction, velocity and thickness.
- Diachronous salt evacuation and passive diapirism along the strike of Nordkapp Basin from NE to SW.
- Rotation of mini-basins due to sediment progradation and far-field stresses is observed.
- Rejuvenation of salt structures during the Triassic–Jurassic transition and early-mid-Eocene.

focus on the following: (i) the interplay between base-salt rift architecture and sediment progradation, (ii) triggering mechanisms for salt mobilisation and rejuvenation of the salt structures and (iii) the distribution and evolution of depocenters together with the formation of depositional fairways and sediment routing patterns associated with salt evacuation from the LES.

The current study provides the concurrent elaboration of the post-salt stratigraphy and tectonic evolution following the study of the deep basin development and the establishment of the pre-salt rift architecture and LES accumulations by Hassaan et al. (2021b) using the same seismic and well data sets. In conjunction, both studies comprise one of the few cases worldwide where improved resolution data sets and integrated analyses contribute to a holistic anatomy of a salt-influenced rift basin.

2 | GEOLOGICAL SETTING

The Paleozoic evolution of the greater Barents Sea has been influenced by the structural fabric of the NW-SE
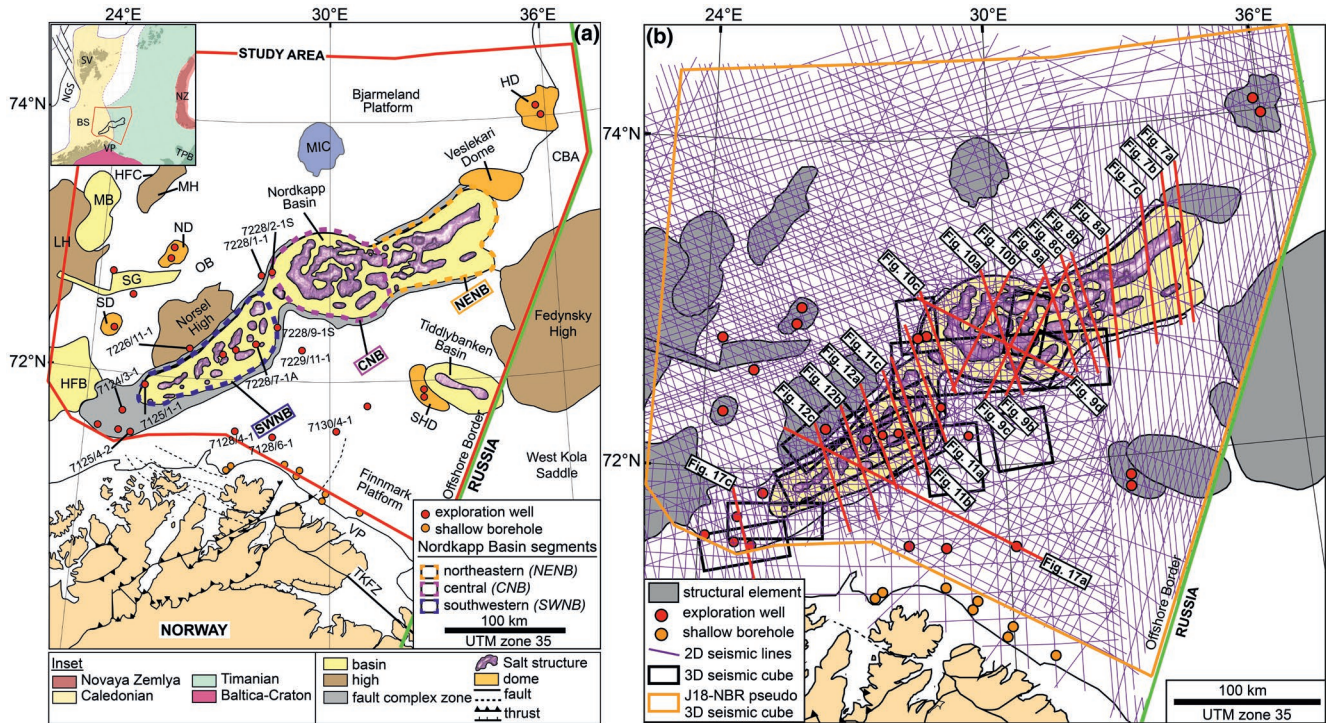
FIGURE 1 (a) Main structural elements of the southwestern and southeastern Norwegian Barents Sea (modified from Hassaan et al., 2020; Mattingsdal et al., 2015) and study area denoted by the red polygon. BS, Barents Sea; CBA, Central Barents Arch; HD, Haapet Dome; HFB, Hammerfest Basin; HFC, Hoop Fault Complex; LH, Loppa High; MB, Maud Basin; MH, Mercurius High; MIC, Mjølnir Impact Crater; ND, Norvarg Dome; NZ, Novaya Zemlya; OB, Ottar Basin; SD, Samson Dome; SG, Swaen Graben; SHD, Signalhorn Dome; Sv, Svalbard; TKFZ, Trollfjorden-Komagelva Fault Zone, TPB, Timan-Pechora Basin; VP, Varanger Peninsula. (b) Used seismic reflection data sets, exploration wells and shallow boreholes (Bugge et al., 1995), overlaid on the main structural elements; study area denoted by red polygon. Seismic data courtesy of NPD and TGS

trending Timanian orogeny of late Neoproterozoic age (e.g. Barrère et al., 2009, 2011; Faleide et al., 2018; Gabrielsen, 1984; Gee et al., 2006; Pease et al., 2016; Schiffer et al., 2020) and by the Caledonian orogeny of Silurian-Devonian age that contributed to NE-SW and NNW-SSE trending basement-inherited structures (e.g. Gernigon & Brönner, 2012; Rice et al., 1989; Roberts, 1972; Roberts & Gee, 1985). Previous studies have proposed that the late Devonian–Mississippian extensional collapse of the Caledonian orogen along the inherited NE-SW to NW-SE basement structures has influenced the development of the Nordkapp Basin (Breivik et al., 1995; Dengo & Røssland, 1992; Faleide et al., 1993, 2008; Gabrielsen et al., 1990; Gernigon et al., 2014; Gudlaugsson et al., 1998; Marello et al., 2013; Ritzmann & Faleide, 2007). The NW-SE trending Carboniferous graben structures in the southeastern Norwegian Barents Sea extend to the CNB and SWNB segments of the Nordkapp Basin following the inherited Timanian structures (Hassaan et al., 2020). Recently, Hassaan et al. (2021b) showed that the spatially variable Timanian- and Caledonian-inherited structures were overprinted by NE-SW oriented late Devonian-early Carboniferous and NW-SE oriented late Carboniferous

extension and gave rise to seven sub-basins separated by interbasin transfer zones in the Nordkapp Basin. During the Pennsylvanian-early Permian, an LES accumulated under warm and arid climate conditions in the Norwegian Barents Sea (Larssen et al., 2002), and it comprises both mobile (i.e. halite) and non-mobile (i.e. anhydrite, carbonates) lithologies (Hassaan et al., 2020, 2021b; Rojo et al., 2019; Rowan & Lindsø, 2017). In the mid-Permian, the shift of depositional environment to temperate conditions allowed the formation of cool-water carbonate platform deposits (Beauchamp, 1994; Stemmerik, 2000).

During the Triassic, regional thermal subsidence conditions prevailed and a prograding system comprising of several cycles of transgressive-regressive marine, deltaic and continental clastic sediments derived from the southeast Urals covered the Barents Sea (Eide et al., 2018; Glørstad-Clark et al., 2010; Klausen et al., 2015). It has been suggested that the salt mobilisation in the Nordkapp Basin was triggered either by early Triassic thick-skinned extension (Jensen & Sørensen, 1992; Koyi et al., 1993, 1995; Nilsen et al., 1995; Rojo et al., 2019; Rojo & Escalona, 2018) and/or by the loading of Triassic progradation towards NW (Dengo & Røssland, 1992; Grimstad, 2016; Rojo

et al., 2019; Rowan & Lindsø, 2017). During the Triassic–Jurassic transition, westward-propagating compressional stress from the evolving Novaya Zemlya fold-and-thrust belt reactivated the Carboniferous structural elements in the Barents Sea (Hassaan et al., 2020, 2021a; Indrevær et al., 2018; Müller et al., 2019). In the Nordkapp Basin, thinning of the lower Cretaceous strata towards the salt diapirs has been associated with structural growth caused by the salt supply from the source layer (Koyi et al., 1993, 1995; Rojo & Escalona, 2018) or as gravity-induced contraction (Nilsen et al., 1995). During the Cenozoic, the Carboniferous structures in the southeastern Norwegian Barents Sea were likely reactivated by far-field stresses propagating from the Eurekan orogeny (Gabrielsen et al., 1997; Gac et al., 2020; Hassaan et al., 2020). Finally, the Cenozoic uplift and related pre-glacial and Plio-Pleistocene glacial erosion have removed most of the late Cretaceous to Cenozoic strata in the Nordkapp Basin (Baig et al., 2016; Henriksen et al., 2011; Lasabuda, Laberg, Knutsen, & Høgseth, 2018; Lasabuda, Laberg, Knutsen, & Safronova, 2018; Rojo et al., 2019; Tsikalas et al., 2012).

3 | DATA AND METHODS

3.1 | Stratigraphic and structural interpretation

The seismic database comprises conventional, 2D, multi-channel, seismic reflection profiles, 12 3D seismic surveys and 1 pseudo-3D seismic cube covering an area of 51,500 km^2 along the studied structural elements the Nordkapp Basin, Norsel High and Veslekari Dome (Figure 1b; Table 1a). An additional surrounding region (95,400 km^2) has been interpreted to comprehend the interplay between the regional tectonics, basin configuration and Triassic progradation. Concerning the reprocessed and the pseudo-3D seismic data sets, it is the first time these become available to academia. The study used sequence stratigraphy principles (Catuneanu et al., 2011), growth strata and reflection termination to understand basin infill history of the Nordkapp Basin. Twelve exploration wells along with shallow boreholes (Bugge et al., 1995) have been used to establish the well-to-seismic ties and time-to-depth conversion and to guide seismic interpretation (Figure 1). The formation well-tops were used to create the litho- and chrono-stratigraphic scheme shown in Figure 2. Twelve seismic sequences bounded by twelve seismic horizons sub-divided the upper Palaeozoic to Cenozoic strata. In particular, the Triassic successions were sub-divided into higher-order chronostratigraphic sequences following the schemes by Glørstad-Clark et al. (2010) and Klausen et al. (2015). Seismic sections

from the reprocessed NBR-CFI and BSSE14-RE seismic surveys (very good/excellent seismic resolution) were used for detailed structural and stratigraphic analyses (Table 1b). The salt structures were interpreted in three dimensions using the multi-z interpretation tool (Petrel v.2019, Schlumberger). Furthermore, regional post-salt time-thickness maps were constructed to illustrate the lateral and vertical configuration of the interpreted stratigraphic sequences, and to compare the tectono-stratigraphic evolution between the Nordkapp Basin and its surrounding regions. The same analysis elucidates the salt evacuation from the different segments over the geological time and its relation to the pre-salt structural configuration.

3.2 | 2D structural restoration and 1D backstripping

Selected seismic sections were converted into depth domain and then used to conduct 2D structural restoration (Move v.2019.1, Petroleum Experts). The depth conversion was based on velocity information from six wells (Table 2) and is associated with some uncertainties due to lack of well ties in the unexplored CNB and NENB Nordkapp Basin segments (Figure 1a). These uncertainties are related to changes in interval velocities caused by lateral lithological variations and diagenesis, and to the less known velocities of deeply buried strata in the mini-basins. The aim of the structural restoration of key seismic sections was to illustrate the temporal post-salt evolution of the Nordkapp Basin. Structural restoration comprised a combination of successive modelling steps. These included decompaction, unfolding by flexural slip, and move-on-fault algorithms to restore the interpreted complex geometries and salt structures, following the established restoration workflows for salt-related deformation by Rowan and Ratliff (2012). Eroded post-Cretaceous strata were reconstructed based on the net erosion estimates for the area by Baig et al. (2016). Within the modelling context, the Bjarmeland and Finnmark platforms were defined as representing regional levels where no significant salt mobilisation occurred due to the presence of non-mobile LES (Hassaan et al., 2021b; Rojo et al., 2019; Rowan & Lindsø, 2017).

In more detail for the performed modelling steps, decompaction was performed by using well-accepted initial porosity, compaction coefficient and sediment grain density parameters for typical lithological (sand, silt, clay) percentages (e.g. Bjørlykke et al., 2004; Mondol et al., 2007; Sclater & Christie, 1980) that were gathered through the available well-log interpretation for each sequence (Table 3). The decompaction step removes the

TABLE 1 (a) Used seismic reflection data sets (TWT, two-way travel time); (b) Calculated vertical seismic resolution for the reprocessed BSSE14RE and CFI-NBR surveys (very good/excellent seismic resolution) that were mainly used for interpretations on selected seismic sections (Figures 7–12) and 2D structural sequential restoration

(a)

Survey	3D/2D	Year	Acquisition company/ authority	Record time (TWT, s)	Study area coverage (3D/km², 2D/km)	Resolution
J18-NBR-3D	Pseudo-3D	2018	TGS	6	ca. 146,900	Very good/excellent
NKFE11	3D	2011	TGS	7	ca. 5,937	Very good/excellent
BG0804	3D	2008	BG Group	5	ca. 652	Very good/excellent
ED16001	3D	2016	Edison Norge	6	ca. 1,514	Good
MC3D	3D	2003	WesternGeco/TGS	4.5	ca. 1,056	Good
SH9102	3D	2010	Norsk Shell	5	ca. 569	Moderate
ST309	3D	2004	Equinor	6.5	ca. 1,954	Good
ST0624	3D	2008	Equinor	12	ca. 836	Moderate
ST0811	3D	2010	Equinor	7.4	ca. 1,077	Good
ST0828	3D	2009	Equinor	4.2	ca. 1,061	Very good/excellent
ST9403	3D	2002	Equinor	5.4	ca. 1,036	Very good/excellent
ST10011	3D	2010	Equinor	6.5	ca. 2,466	Moderate
ST10012	3D	2011	Equinor	4.5	ca. 667	Very good/excellent
BSSE14-RE	2D	2014	NPD/TGS	9	ca. 18,305	Very good/excellent
CFI-NBR	2D	2018	TGS	10	ca. 28,270	Very good/excellent
NPD-BA-11	2D	2011	NPD	9	ca. 18,305	Moderate
IS-CNB-01	2D	2001	Inseis AS	8	ca. 2,966	Good
IS-CNBE-06	2D	2006	Inseis AS	9.8	ca. 535	Good
NBR-06	2D	2006	NPD	10	ca. 4,245	Moderate
NBR-07	2D	2007	NPD	10	ca. 4,560	Moderate
NBR-08	2D	2008	NPD	10	ca. 9,330	Moderate
NBR-09	2D	2009	NPD	10	ca. 4,650	Moderate
NBR-10	2D	2010	NPD	10	ca. 2,690	Moderate
NBR-12	2D	2012	NPD	10	ca. 9,825	Good
NBR-14	2D	2014	NPD	6	ca. 7,200	Moderate
BARE-02	2D	2002	NPD/TGS	6	ca. 4,785	Poor
BARE-05	2D	2005	NPD	6	ca. 2,405	Poor
BSS01	2D	2001	TGS	8	ca. 4,967	Moderate
TTR84R1	2D	1984	NPD	6	ca. 2,938	Moderate

(b)

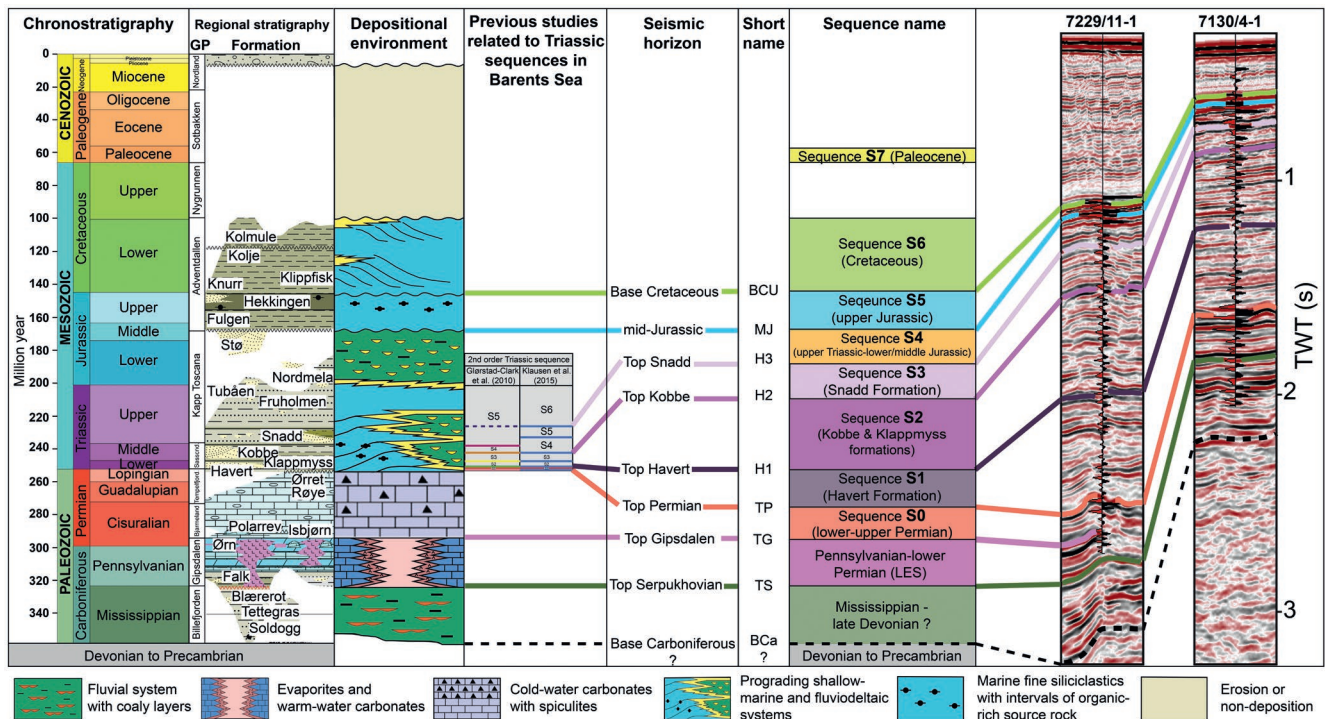| Zone		Frequency (Hz) (F)	Interval velocity (m/s) (V)	Wavelength (m) (λ = V/F)	Vertical resolution (m) (λ/4)
Shallow	Cretaceous to Jurassic	50	2,335	47	12
Intermediate	Triassic	30	4,000	133	33
Deep	Permian to Pennsylvanian	15	6,280	419	105
		20	6,280	314	79
	Mississippian	15	4,960	331	83
		20	4,960	248	62

FIGURE 2 Stratigraphic framework and key seismic horizons interpreted throughout the study area based on twelve exploration wells (Figure 1). Regional stratigraphy and depositional environment scheme is based on Larssen et al. (2002) modified after Gernigon et al. (2018) and Rojo et al. (2019) and geologic timescale after Gradstein and Ogg (2020). GP: (stratigraphic) group. The seismic-stratigraphic framework is also tied to earlier chrono-stratigraphic schemes for Triassic successions by Glørstad-Clark et al. (2010) and Klausen et al. (2015). TWT, two-way travel time

effect of burial compaction through time and displays the temporal variations in sequence thickness. The modelling incorporated Airy isostatic compensation during each decompaction step to quantify and remove the effects of differential loading and basin subsidence on the basement adjustments. Subsequently, the decompacted strata were unfolded to the regional level by using the flexural slip algorithm (Move v.2019.1, Petroleum Experts). Paleo-water depths were not included in the modelling due to lack of relevant data in the NENB and CNB segments. Nevertheless, paleo-water depth levels were calculated to be <300 m within the Nordkapp Basin (Rojo et al., 2019) and, thus, accompanying maximum errors resulting from neglecting palaeowater depths in the modelling are of the same order.

1D backstripping was performed on the selected locations at the Finnmark and Bjarmeland platforms, and within the Nordkapp Basin segments (i.e. NENB, CNB and SWNB) to estimate the paleo-thicknesses and paleo-sediment accumulation rates of the sequences S1–S5. The sedimentation rate curves help to establish a link between the regional progradation and sediment accumulation and to illustrate the differences between the sediment accumulation on the margin and interior basin. The curve fluctuations within the individual basin

segment highlight the mini-basins subsidence processes that were strongly influenced by salt tectonics. The present-day thicknesses of the post-salt sequences were gathered by using the same depth converted seismic sections for 2D sequential structural restoration. Similarly, the addition of eroded post-Cretaceous strata is based on the net erosion estimates by the Baig et al. (2016). The input mechanical compaction parameters (i.e. initial porosity, compaction coefficient and sediment grain density) are based on the lithological interpretation of each sequence (Tables 2 and 3). The sediment accumulation rate of the sequences S1–S5 were calculated as the paleo-thickness (decompacted) divided by the depositional age (Myr) of the individual sequence (S1-2.1, S2-8.3, S3-26.5, S4-50 and S5-20 Myr).

4 | RESULTS

4.1 | Basin configuration and salt structures

In this section, we provide a brief overview of the established deep basin configuration and salt structure characteristics as elucidated by Hassan et al. (2021b);

Figure 3 illustrates the established abbreviations and informal naming (Table 4). The overview provides the seamless connection to the post-salt evolution of the Nordkapp Basin worked out in this study. The Nordkapp Basin evolved over heterogeneous basement composition and topography as revealed by the available magnetic data (Gernigon et al., 2018; Hassaan et al., 2021b). The so-called Middle Allochthon Front represents an amalgamation of thrust units and separates the contrasting Timanian and Caledonian inherited structures at the CNB Nordkapp Basin segment (Figure 4a; Hassaan et al., 2021b). The rheological properties, locations, orientations and interaction between the Timanian and Caledonian inherited structures promoted the zones of weakness that controlled the basin initiation during the late Devonian-early Carboniferous and late Carboniferous extensional phases (Hassaan et al., 2021b). The base-salt surface at Top Serpukhovian level shows distinct structural relief in the different segments (NENB, CNB and SWNB) of the Nordkapp Basin (Figure 3a). The three segments are separated by the northern transfer zone (NTZ) and southern transfer zone (STZ) and are further subdivided into seven sub-basins SB1-7 (Figure 3b). The evolution of the Nordkapp Basin is controlled by the NW–SE, E–W and NE-SW striking master faults, structural highs and basin boundary fault complexes (Figure 3b; Hassaan et al., 2021b). It is noteworthy that the configuration of the structural highs defines the location and orientation of the post-salt depocenters (Hassaan et al., 2021b; Pichel et al., 2019). The base-salt surface is shallow in sub-basins SB1 and SB4-7 in contrast to sub-basins SB2-3 (Figure 3a).

The multi-z salt model at top Gipsdalen (Figure 2) level illustrates the distribution of the salt structures in the Nordkapp Basin. These structures display a wide range of orientations, sizes, shapes and lateral extent and are largely controlled by pre-salt structural highs and lows (or topography) (Figure 3c; Table 4; Hassaan et al., 2021b). The distinct post-salt structural features, which include turtle structures, secondary welds, collided and dwarf secondary mini-basins, salt wings and megaflaps are all associated to the salt structures (Figure 3c), as defined in other salt-bearing basins worldwide (Jackson & Hudec, 2017). In detail, the NENB segment contains the most extensive salt wall (SS1) in the basin, which also contains physically linked and isolated salt structures (e.g. SS2-7). The CNB segment contains the most prominent, irregularly shaped and voluminous salt structure of the Nordkapp Basin, informally termed the Dragon foot (DF) salt structure (based on its planform geometry; Hassaan et al., 2021b) along with other linked and scattered salt structures (e.g. SS8-12). The SS13 salt structure is located above the antithetic interbasin ridge (STZ). It is noteworthy that the salt structures SS14–30 in the SWNB segment are scattered.

The estimated present-day evacuated mobile salt from the LES is thickest (ca. 4.4 km) in the SB2-3 sub-basins. Sub-basin SB4 contains the least (ca. 0.9 km) evacuated mobile salt, whereas sub-basins SB5-7 hold less mobile (ca. 0.9–1.6 km) and thick residual LES (Figure 3c; Hassaan et al., 2021b).

4.2 | Post-salt sequences

The post-salt seismic stratigraphy is highly variable and complex within the Nordkapp Basin. Salt diapirism, extension, contraction and regional uplift affected the lower-upper Permian to Cenozoic strata. Below, we describe the detailed post-salt seismic stratigraphy, distinct geometries formed by salt–sediment interaction, salt evacuation, major sediment depocenters and paleo-sediment accumulation rates based on isochron-thickness maps (Figure 5), 1D backstripping (Figure 6) and a series of interpreted seismic sections (Figures 7–12).

4.2.1 | Lower-upper Permian (sequence S0)

The lower-upper Permian sequence S0 consists of successions belonging to the Bjarmeland and Tempelfjorden groups (Figure 2). Overall, the sequence is thin (ca. 105 ms twt/two-way travel time) in the NENB segment and above the Veslekari Dome, while it is upturned near the salt structures and is truncated by the lowermost Triassic sequence S1 (Figures 4b, 7 and 8). Sequence S0 appears to be tabular and homogeneous, and occasionally local thickness variations can be observed on the Bjarmeland and Finnmark platforms near the carbonate build-ups. The sequence is gradually thickening (ca. 190–290 ms twt) towards SW in the CNB and SWNB segments (Figures 9–12). It is noteworthy that sequence S0 is thick within local depocenters and is thin and upturned in the proximity of salt structures in the SWNB segment (Figures 11b,c and 12). The regional thickness map shows variations south of the Middle Allochthon Front within the CNB and SWNB segments (Figure 4b).

4.2.2 | Lowermost Triassic (sequence S1)

The lowermost Triassic sequence S1 consists of the siliciclastic sediments of the Havert Formation (Induan). On a regional scale, the sediments thin from the east (ca. 1,000 ms twt) to the SW (ca. 400 ms twt) and NW (ca. 100 ms twt) within the study area (Figures 2 and 5a). The regional progradation from the east seems to interfere with sediments prograding from mainland Norway

IAS EAGE –WILEY |

TABLE 2 Calculated average and interval velocity for depth conversion of the selected seismic sections (OWT, one-way travel time; TWT, two-way travel time). For sequence and horizon names, refer to Figure 2

Formation tops and sequence	7124/3-1				7226/11-1				7228/2-1				7228/1-1				7228/9-1				7229/11-1					
	Depth (m)	Thickness (m)	OWT (ms)	TWT (ms)	Depth (m)	Thickness (m)	OWT (ms)	TWT (ms)	Depth (m)	Thickness (m)	OWT (ms)	TW (ms)	Depth (m)	Thickness (m)	OWT (ms)	TWT (ms)	Depth (m)	Thickness (m)	OWT (ms)	TWT (ms)	Depth (m)	Thickness (m)	OWT (ms)	TWT (ms)	Average velocity (m/s)	Interval velocity (m/s)
Top Nordland (Seabed)	272			367	237			432	349			494	351			512	278			430	283			414	1,470*	
Cretaceous		925	367			886	359			746	307			489	188			728	287			904	386			2,490
Top Hekkingen (BCU)	1,197			1,102	1,123			1,150	1,095			1,108	840			887	1,006			1,003	1,187			1,187	2,000	
Upper Jurassic		48	14			47	26			96	38			47	19			43	16			83	19			2,850
Top Stø (Middle Jurassic)	1,245			1,130	1,170			1,201	1,191			1,183	887			924	1,049			1,034	1,270			1,224	2,030	
Sequence S4 (Upper Triassic–Lower/Middle Jurassic)		145	30			102	46			227	65			209	67			159	51			158	46			3,310
Top Snadd	1,390			1,189	1,272			1,292	1,418			1,312	1,096			1,058	1,208			1,136	1,428			1,316	2,140	
Sequence S3 (Snadd formation)		431	168			582	108			838	215			375	110			363	105			390	132			3,520
Top Kobbe	1,821			1,524	1,854			1,507	2,256			1,743	1,471			1,279	1,571			1,345	1,818			1,580	2,400	
Sequence S2 (Kobbe and Klappmyss formations)		737	288			1,035	244			1,275	338							1,030	278			962	214			3,690
Top Havert	2,558			2,100	2,889			1,995	3,531			2,419					2,601			1,901	2,780			2,009	2,750	
Sequence S1 (Havert formation)		773	228			964	246										1,173	284			1,073	186			4,225
Top Ørret (Top Permian)	3,331			2,556	3,853			2,486									3,774			2,468	3,853			2,381	3,000	
Middle-upper Permian		763	87			455	68										446	94			402	144			5,300
Top Ørn (Top Salt)	4,094			2,729	4,308			2,622									4,220			2,656	4,255			2,669	3,150	
Pennsylvanian-early Permian (syn- to early post-rift LES)																										4,500
Mississippian–late Devonian?																										5,500
Devonian–Precambrian																										6,000

TABLE 3 Interpreted lithologies from well logs that were used to estimate decompaction parameters for the 2D structural sequential restoration and 1D backstripping. For sequence and horizon names, refer to Figure 2

Rock type or lithology	Sandstone	Shale	Limestone	Salt
Initial porosity, φ_0 (fraction)	0.49	0.63	0.51	0
Compaction coefficient, c (km^{-1})	0.27	0.51	0.52	0
Mean density of grains, ρ (kg/m^3)	2,650	2,720	2,710	2,160

		Lithology percentage (%)				Final decompaction parameters		
Horizon	Sequence	Sandstone	Shale	Limestone	Salt	Total φ_0 (fraction)	Total c (km^{-1})	Total ρ (kg/m^3)
Top Nordland (Seabed)	Sequence S7 (Paleocene)	10	90	0	0	0.62	0.50	2,713
Top Kolmule (Seabed)	Sequence S6 (Cretaceous)	20	80	0	0	0.6	0.49	2,706
Top Hekkingen (BCU)	Sequence S5 (Upper Jurassic)	0	100	0	0	0.63	0.51	2,720
Top Stø (middle Jurassic)	Sequence S4 (Upper Triassic–Lower/Middle Jurassic)	80	20	0	0	0.52	0.41	2,664
Top Snadd	Sequence S3 (Snadd formation)	50	50	0	0	0.56	0.45	2,685
Top Kobbe	Sequence S2 (Kobbe and Klappmyss formations)	50	50	0	0	0.56	0.45	2,685
Top Havert	Sequence S1 (Havert formation)	20	80	0	0	0.60	0.49	2,706
Top Ørret (Top Permian)	Middle-upper Permian	0	0	100	0	0.51	0.52	2,710
Top Ørn (Top Salt)	Pennsylvanian-early Permian (syn- to early post-rift LES)	0	0	0	100	0	0	2,160
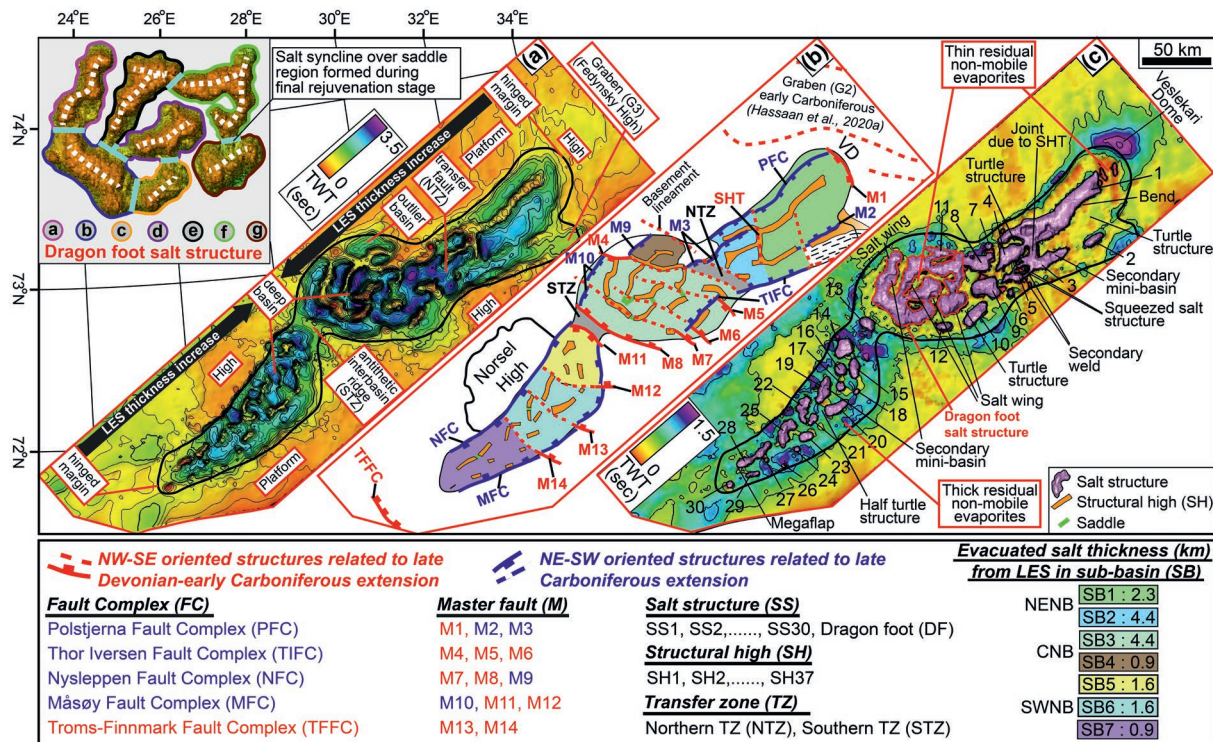
FIGURE 3 Deep basin configuration and salt structure characteristics with established abbreviations and informal naming (modified from Hassaan et al., 2021b). (a) Time-thickness map (TWT, two-way travel time, ms) between the base-salt (top Serpukhovian) and regional level (based on Bjarmeland and Finnmark platforms) shows Pennsylvanian-early Permian LES accumulations controlled by pre-salt rift architecture before the salt mobilisation. (b) Master faults and structural highs arrangement. Sub-basins SB1-7 are illustrated with different colour rasters. Abbreviations refer to structural features shown in the legend and described in the text. (c) TWT (two-way travel time, ms) between the base-salt (top Serpukhovian) and top-salt (top Gipsdalen) displays salt evacuation from the Pennsylvanian-early Permian LES, salt structures and residual non-mobile evaporites in the different segments of the Nordkapp Basin. SHT, structural high Timanian. Inset, zoom-in of the Dragon foot (DF) salt structure showing its different segments (a–g)

in the south (Figure 5a; Eide et al., 2018; Glørstad-Clark et al., 2010). Within the Nordkapp Basin, sequence S1 shows drastic thickness variations (Figures 5a and 7c).

Adjacent to the NENB segment, the sediment accumulation rates for sequence S1 show slight variations on the Finnmark (ca. 1,100–1,092 m/Myr) and Bjarmeland (ca. 1,019–1,146 m/Myr) platforms from the NE to the SW. However, a clear contrast can be observed within the NENB segment as the sediment accumulation rates increase sharply (ca. 1,366–2,479 m/Myr) (Figure 6a; Table 5a). Sequence S1 exhibits isopachous thickness over the Finnmark Platform and is characterized by parallel to inclined reflections that are offset by an NNW-dipping post-salt normal fault overlying an NE-SW oriented salt anticline (Figure 7a). Towards the axis of sub-basin SB1, sequence S1 forms a turtle structure, whereas the thickness seems to be unaffected over the Veslekari Dome (Figure 7b). Farther SW, sequence S1 thickens dramatically as evidenced by the formation of growth strata and shifting depocenters towards the NNW (Figure 7c). Within sub-basin SB2, three collided mini-basins separated by

secondary welds are prominent. A thick-skinned NNW-dipping reverse fault along a secondary weld separates two of the collided mini-basins and reaches the seafloor (Figure 8b, red arrow). The central mini-basin is bounded by the two secondary welds and shows growth strata towards the NW, which led to the also accommodation of layers and wedge-shaped mini-basin strata in the lower and upper parts, respectively (Figure 8b). Farther to the SW, the mini-basin is rotated (around a horizontal axis) with southeastward tilt and shows bowl- and wedge-geometry (Figure 8c) (Jackson et al., 2020). The internal packages of sequence S1 thicken towards NW against SS4 salt wall, whereas thinning and being truncated against the other side (Figure 8c).

Adjacent to the CNB segment, the sediment accumulation rates of sequence S1 are higher over the Bjarmeland Platform (ca. 1,146–1,182 m/Myr) than the Finnmark Platform (ca. 1,058–1,125 m/Myr). Overall, the CNB segment seems to be a transition region between the NENB and SWNB segments as sediment accumulation rates gradually decrease towards the SW (ca. 1,164–2,639 m/Myr)

TABLE 4 Structural characteristics of the salt structures in the three Nordkapp Basin segments: northeastern (NENB), central (CNB) and southwestern (SWNB)

(a) Northeastern Nordkapp segment (NENB)

Salt structure (SS)	Shape of SS	Lateral extent (km)		Axial ratio	Type of SS	Orientation
		Length	Width			
1	Elongated	ca. 81	ca. 13.2 (SW), ca. 10.4 (NE)	6.86	Wall	NW–SE
2	Elongated	ca. 14.4	ca. 4.6	3.13	Wall	NW–SE
3	Elongated	ca. 27.7	ca. 7.6	3.64	Wall	NW–SE
4	Elongated	ca. 24.7	ca. 8.6	2.87	Wall	NW–SE
5	Sub-circular	ca. 8.5	ca. 5.2	1.63	Stock	
6	Circular	ca. 5.1	ca. 3.3	1.55	Stock	
7	Circular	ca. 5	ca. 4.9	1.02	Stock	

(b) Central Nordkapp segment (CNB)

Salt structure (SS)	Shape of SS	Lateral extent (km)		Axial ratio	Type of SS	Orientation
		Length	Width			
8	Sub-circular	ca. 17.6	ca. 16.3	1.08	Stock	
9	Sub-circular	ca. 17.2	ca. 13.6	1.26	Stock	
10	Elongated	ca. 20.5	ca. 7.6	2.70	Wall	NW–SE
11	Elongated	ca. 14.3	ca. 6.8	2.10	Wall	E–W
12	Sub-circular	ca. 10.1	ca. 5.5	1.84	Stock	
Dragon foot (DF)	Branched	a: ca. 26.6	a: ca. 9.8	a: 2.71	Connected salt walls and stock	a: NNE–SSW
		b: ca. 27.6	b: ca. 11.6	b: 2,38		b: NW–SE
		c: ca. 19.3	c: ca. 7.1	c: 2.72		c: NW–SE
		d: ca. 24.9	d: ca. 8.1	d: 3.07		d: NW–SE
		e: ca. 33.4	e: ca. 8.6	e: 3.88		e: NNE–SSW
		f: 23.2 (E–W) + 20.4 (NW–SE) = ca. 43.6	f: ca. 7.4	f: 5.89		f: E–W to NW–SE
		g: ca. 19.9	g: ca. 13.3	g: 1.50		g: NW–SE
13	Sub-circular	ca. 11.2	ca. 6.9	1.62	Stock	

(c) Southwestern Nordkapp segment (SWNB)

Salt structure (SS)	Shape of SS	Lateral extent (km)		Axial ratio	Type of SS	Orientation
		Length	Width			
14	Sub-circular	ca. 12.1	ca. 8.5	1.42	Stock	
15	Elongated	ca. 11.4	ca. 4.1	2.78	Wall	N–S
16	Sub-circular	ca. 5.7	ca. 4.9	1.16	Stock	
17	Sub-circular	ca. 5.2	ca. 4.7	1.11	Stock	
18	Circular	ca. 4.4	ca. 3.1	1.42	Stock	
19	Elongated	ca. 20.1	ca. 4.2	4.79	Wall	NW–SE
20	Elongated and elliptical	ca. 17.6	ca. 4.2	4.19	Wall	NW–SE
21	Sub-circular	ca. 8.7	ca. 5.1	1.71	Stock	

(Continues)

TABLE 4 (Continued)

(c) Southwestern Nordkapp segment (SWNB)

Salt structure (SS)	Shape of SS	Lateral extent (km)		Axial ratio	Type of SS	Orientation
		Length	Width			
22	Elongated	ca. 18.6	ca. 3.8	4.89	Wall	N–S
23	Elongated	ca. 9.7	ca. 5.8	1.67	Stock	ENE–WSW
24	Sub-circular	ca. 4.3	ca. 4.0	1.08	Stock	
25	Elongated and elliptical-L	17.8 (N–S) + 9.9 (E–W) = ca. 27.7	ca. 5	5.54	Wall	N–S to E–W
26	Sub-circular	ca. 2.7	ca. 2.4	1.13	Stock	
27	Sub-circular	ca. 3.1	ca. 2.6	1.19	Stock	
28	Elongated	ca. 27.8	ca. 4.6	6.04	Wall	NW–SE
29	Elongated	ca. 9.1	ca. 3.1	2.94	Wall	NW–SE
30	Sub-circular	ca. 5.2	ca. 4.6	1.13	Stock	
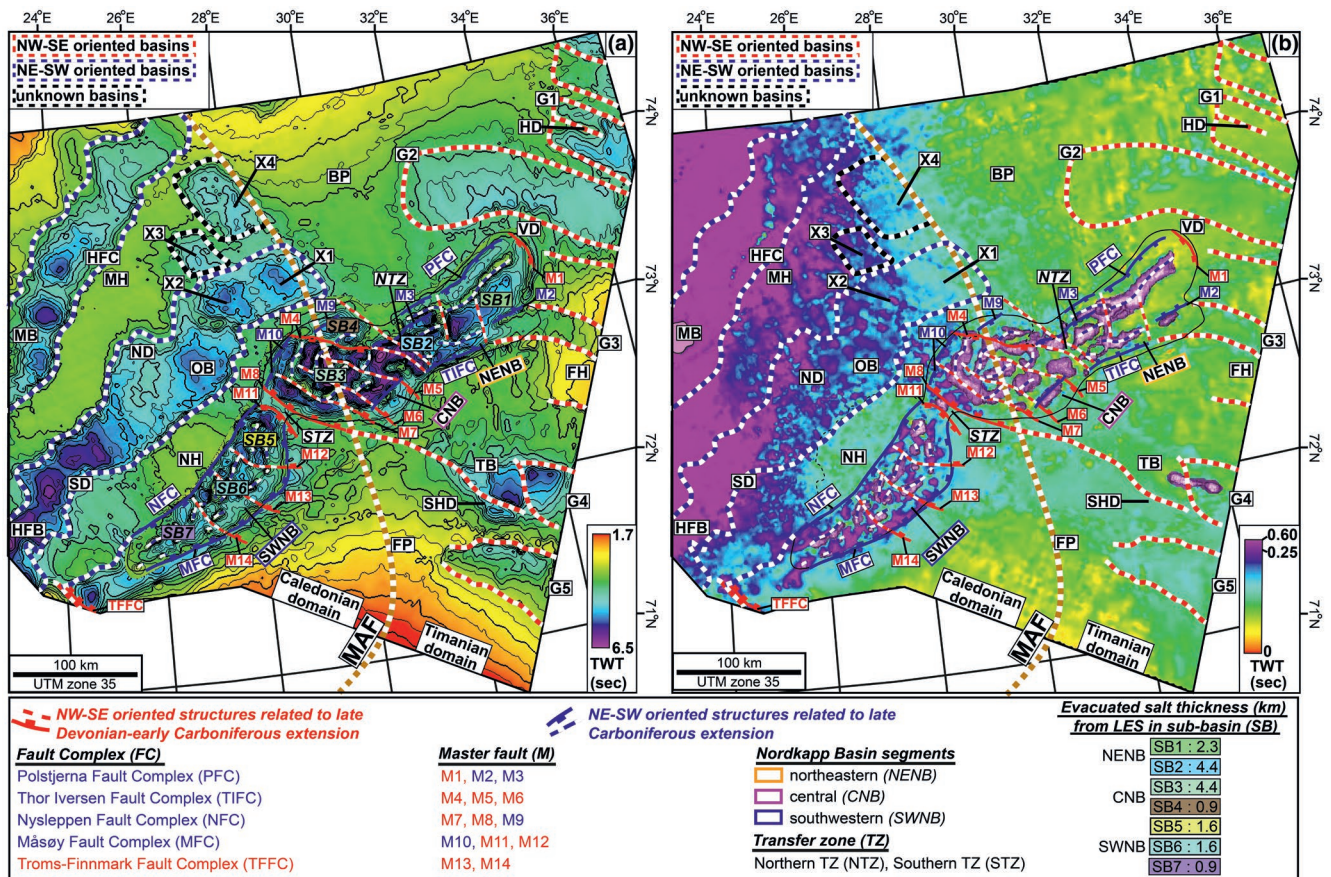
FIGURE 4 (a) Time-structure map at the Top Serpukhovian (TS) level for the Nordkapp Basin and base Carboniferous (BCa?) level for the surrounding region illustrating the regional structural configuration. (b) Regional thickness map (TWT, two-way travel time, s) of the lower-upper Permian sequence S0 overlaid with the structural configuration based on seismic interpretation in the southeastern and southwestern Barents Sea. X1-4: newly interpreted/inferred basins (Hassaan et al., in review). BP, Bjarmeland Platform; FH, Fedynsky High; FP, Finnmark Platform; G, Graben; MAF, Middle Allochthon Front; NH, Norsel High; TB, Tiddlybanken Basin; VD, Veslekari Dome. Other abbreviations as in Figure 1. Figure modified from Hassaan et al. (in review)

(Figures 5a and 6a; Table 5b). Generally, sequence S1 is thicker in sub-basin SB3 in comparison with sub-basin SB4. Internally, sequence S1 shows bowl and wedge successions that are partly eroded to the southeast and onlapping growth strata to the NW in the northeastern part of the CNB segment in the sub-basin SB1 (Figure 9b1; Jackson et al., 2020). The SS12 salt stock forms exactly above the thick-skinned NNE-dipping M7 normal fault and influences the thickness of sequence S1 (Figure 9b,c). Few mini-basins in the CNB segment are also rotated (around a horizontal axis) and

tilted to various directions along with overburden sediment accumulation variations (Figures 9b,d and 10a). Sequence S1 shows isopachous geometry with minor thickness variations and is offset by post-salt faults within the CNB segment, in contrast to the platform regions (Figure 10c).

Adjacent to the SWNB segment, the sediment accumulation rates of sequence S1 decrease from the Bjarmeland Platform (ca. 953 m/Myr) to the Norsel High (ca. 878 m/Myr), but they are overall higher in comparison with the ones in the Finnmark Platform (ca. 749–792 m/Myr)
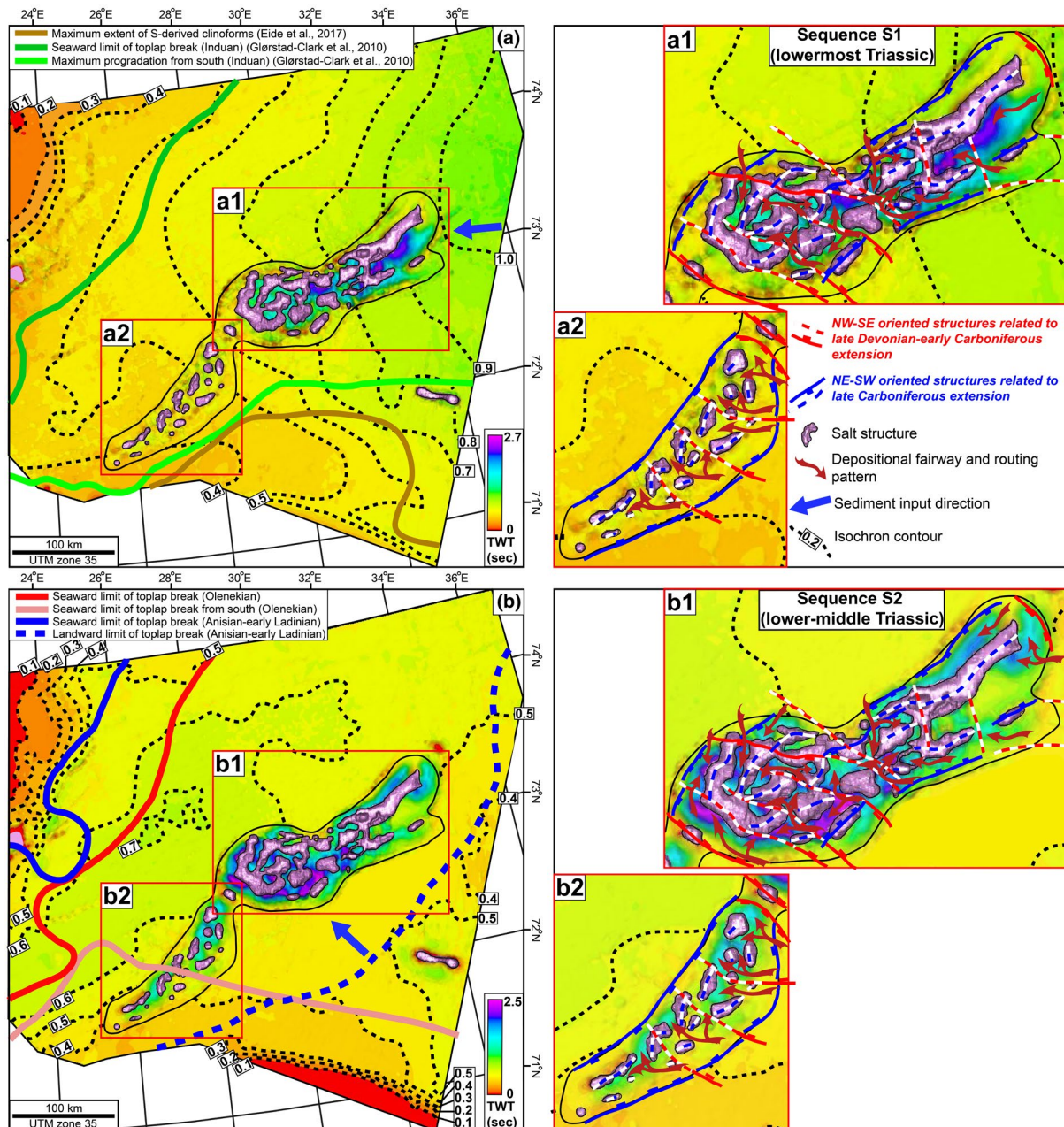
FIGURE 5 Time-thickness maps of: (a) lower Triassic sequence S1, (b) lower-middle Triassic sequence S2, (c) upper Triassic sequence S3 and (d) upper Triassic-BCU sequence S4 and S5. Maps display regional thickness trends of the prograding sediments in Barents Sea, and depocenter variations and salt evacuation within the Nordkapp Basin. Seaward and landward limits are based on the Glørstad-Clark et al. (2010)
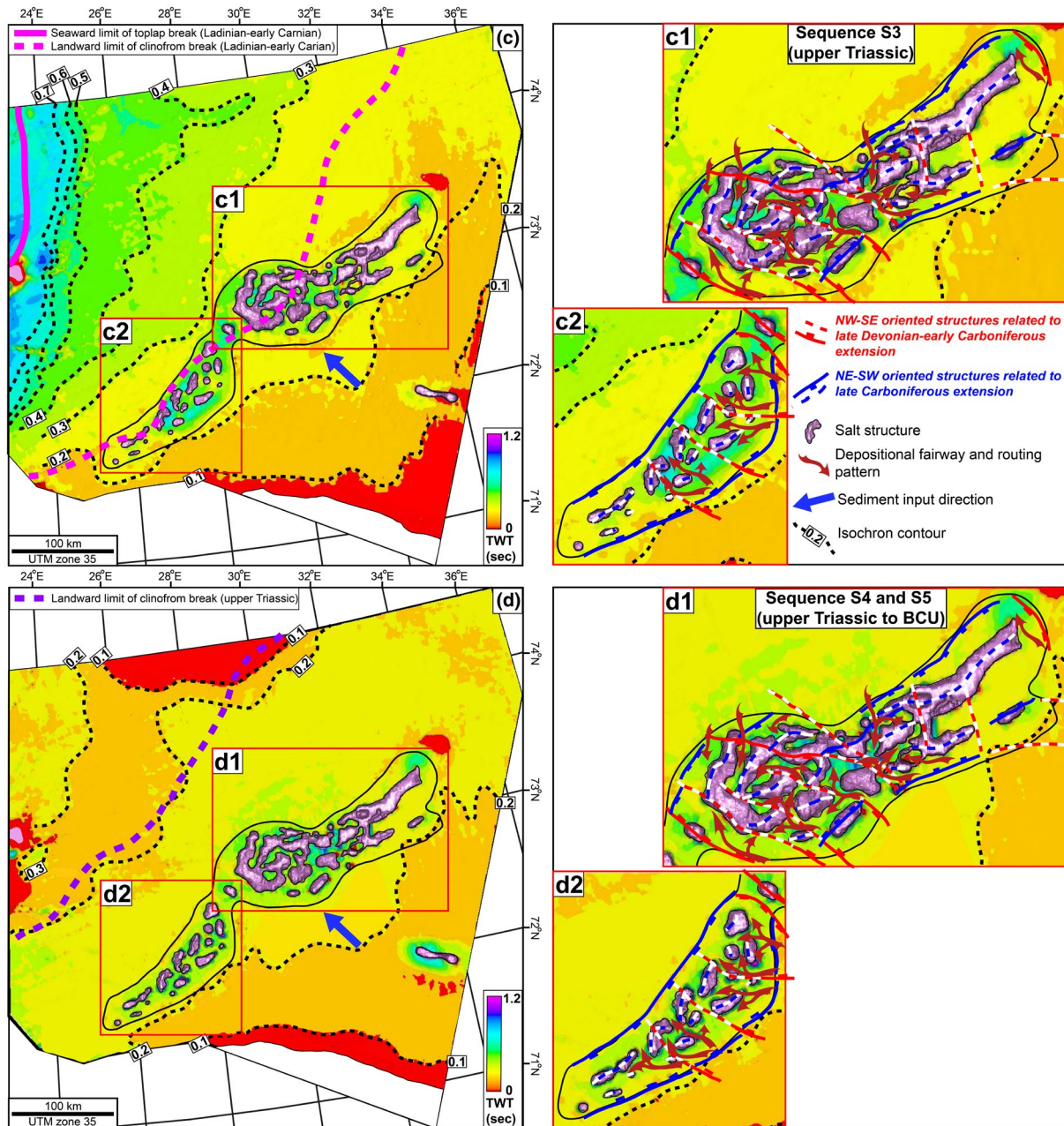
FIGURE 5   (Continued)

(Figures 5a and 6a; Table 5c). Sequence S1 is isopachous across the Bjarmeland Platform, the Norsel High and the Finnmark Platform with only slight thickness variations (Figures 11 and 12). Occasionally, sequence S1 is offset by the thick-skinned Nysleppen Fault Complex (Figures 11a and 12c) but is mostly penetrated by post-salt marginal faults that are decoupled by the thick LES from the thick-skinned Måsøy and Nysleppen fault complexes. Internally within the SWNB segment, sequence S1 thins and onlaps the upturned sequence S0 and becomes thicker in the local depocenters around the salt structures (Figures 2a and 11c). The sediment

accumulation rates are variable in the individual depocenters with a gradual decrease from NE (ca. 1,245 m/Myr) to SW (ca. 999 m/Myr). The prominent upturned strata are situated along the SS18 salt stock and SS20 salt wall, which is more open towards NE and is confined to the SW by the asymmetrical sediment infill across these salt structures (Figure 11b,c). The upturned sequence S1 is 8 km wide and thins along the flank of the SS18 salt stock where it reaches to depth of ca. 1,915 ms twt. An expulsion rollover structure related to salt dynamics is formed along the SS19 salt wall that tilts slightly to the southeast. Internally, the reflections of sequence S1
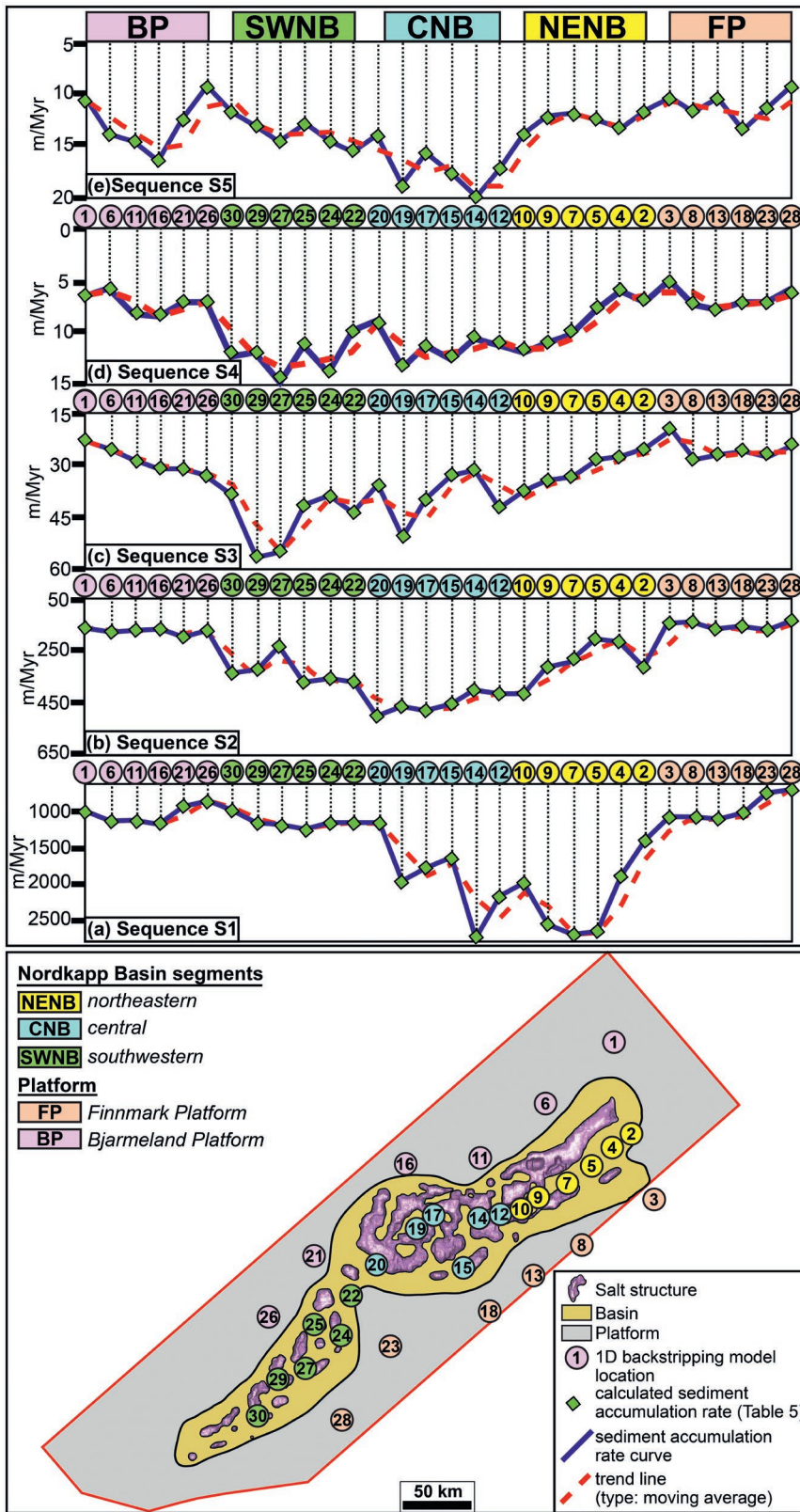
FIGURE 6 Compiled curve plots (a–e for sequences S1–S5, respectively; cf. Figure 2) for sediment accumulation rate variations of the deposited lower Triassic to middle Jurassic successions within the Nordkapp Basin NENB, CNB and SWNB segments, and on the Finnmark (FP) and Bjarmeland (BP) platforms. Numbers (1–30) with different colours represent locations where 1D backstripping models of sediment accumulation rates were calculated on selected seismic sections (Table 5, locations/points 1–30)

onlap the upturned sequence S0 towards NW along the SS19 salt wall (Figure 12a). To the southeast, sequence S1 is offset by a NW dipping post-salt fault that seems to be associated with the pre-salt structural high SH27 (Figure 12a).

4.2.3 | Lower-middle Triassic (sequence S2)

The lower-middle Triassic sequence S2 is comprising siliciclastic successions of the Klappmyss and Kobbe formations (Olenekian to early Ladinian) and thickens regionally
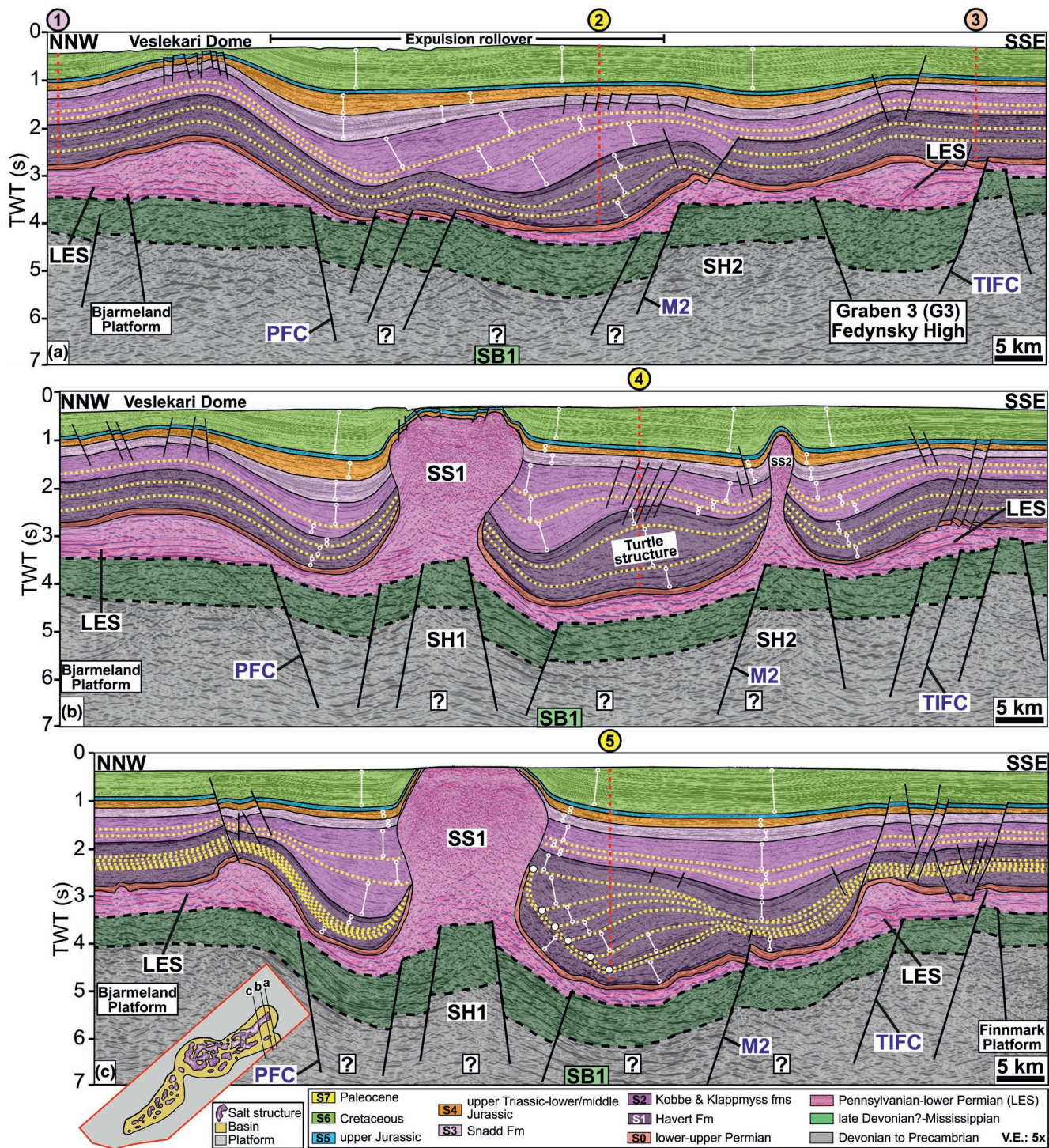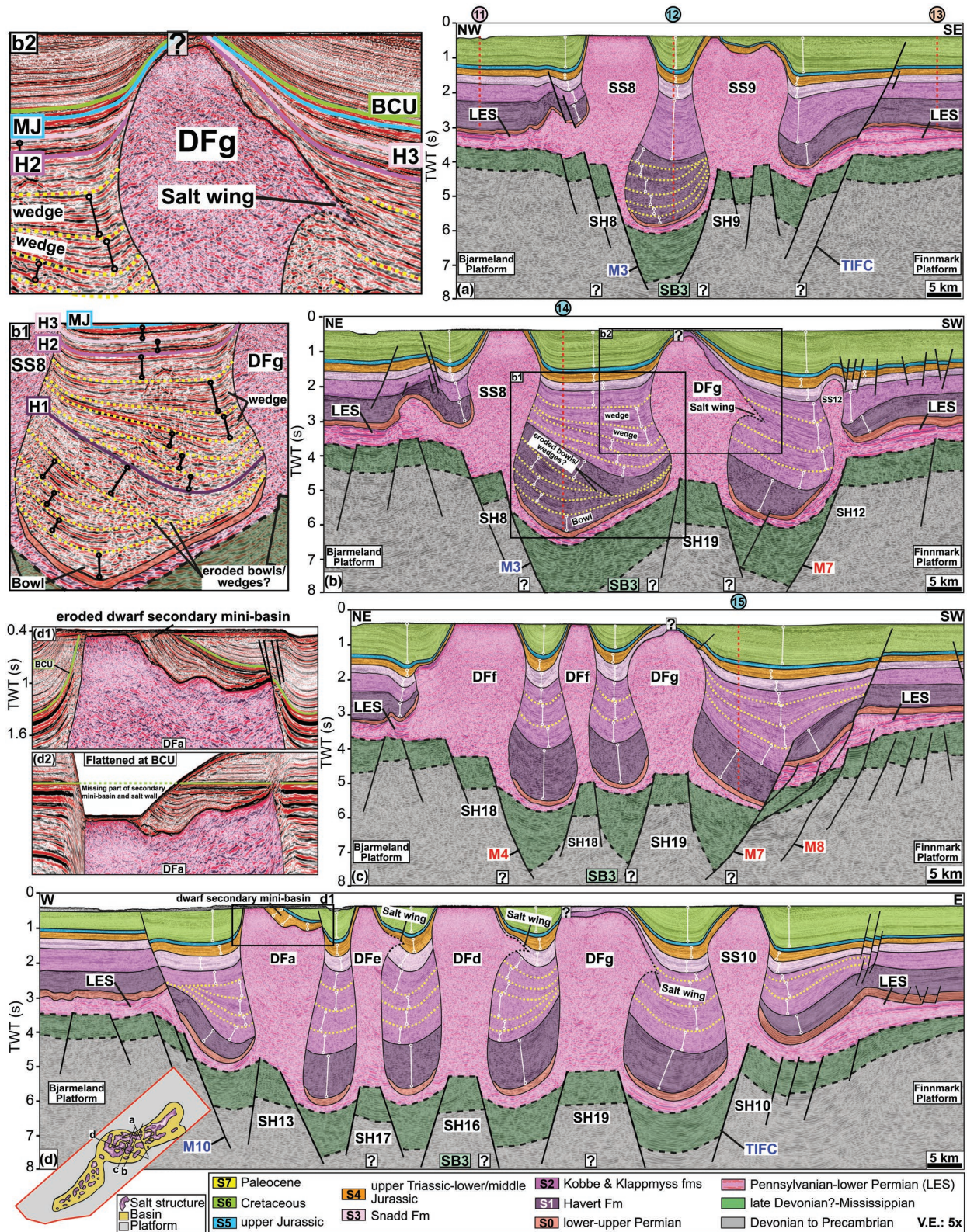
FIGURE 7 (a–c) Interpreted seismic sections (TWT, two-way travel time, s; vertical exaggeration: 5×) illustrating pre-evaporite geometries, layered evaporite sequence (LES), salt structures and post-salt sedimentation patterns in the northeastern (NENB) Nordkapp Basin segment. M, Master fault; PFC, Polstjerna Fault Complex; SB, sub-basin; SH, structural high TIFC, Thor Iversen Fault Complex. Colour-rasters correspond to interpreted sequences in Figure 2. Open white circles connected by white lines display the thickness variations and salt structures (SS) as in Figure 3c. Numbers 1–5 denote the locations of 1D backstripping models that were used to calculate sediment accumulation rates as in Figure 6 and Table 5. Profile locations also in Figure 1b. Seismic data courtesy of NPD and TGS

(ca. 700 ms twt) towards the Bjarmeland Platform across the Nordkapp Basin and then thins (ca. 100 ms twt) farther towards NW (Figures 2, 5b and 6b). During Olenekian,

the sediment progradation from the east was affected by the sediment input from mainland Norway in the south (Figure 5b; Glørstad-Clark et al., 2010). The time-thickness
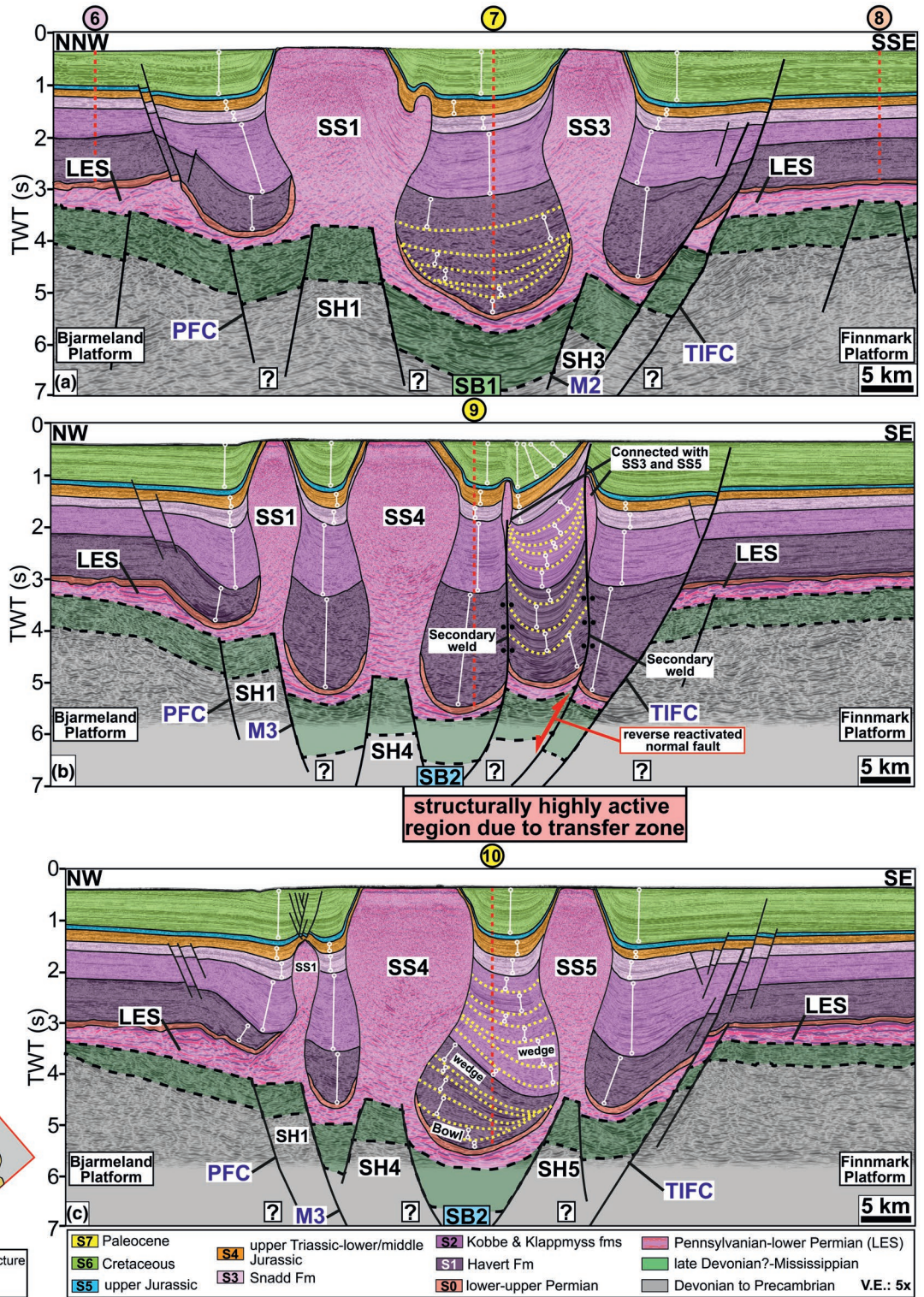
FIGURE 8 (a–c) Interpreted seismic sections (TWT, two-way travel time, s; vertical exaggeration: 5×) illustrating pre-evaporite geometries, layered evaporite sequence (LES), salt structures and post-salt sedimentation patterns in the northeastern (NENB) Nordkapp Basin segment. M, Master fault; PFC, Polstjerna Fault Complex; SB, Sub-basin; SH, Structural high; TIFC, Thor Iversen Fault Complex. Colour-rasters correspond to interpreted sequences in Figure 2. Open white circles connected by white lines display the thickness variations and salt structures (SS) as in Figure 3c. Numbers 6–10 denote the locations of 1D backstripping models that were used to calculate sediment accumulation rates as in Figure 6 and Table 5. Profile locations also in Figure 1b. Seismic data courtesy of NPD and TGS
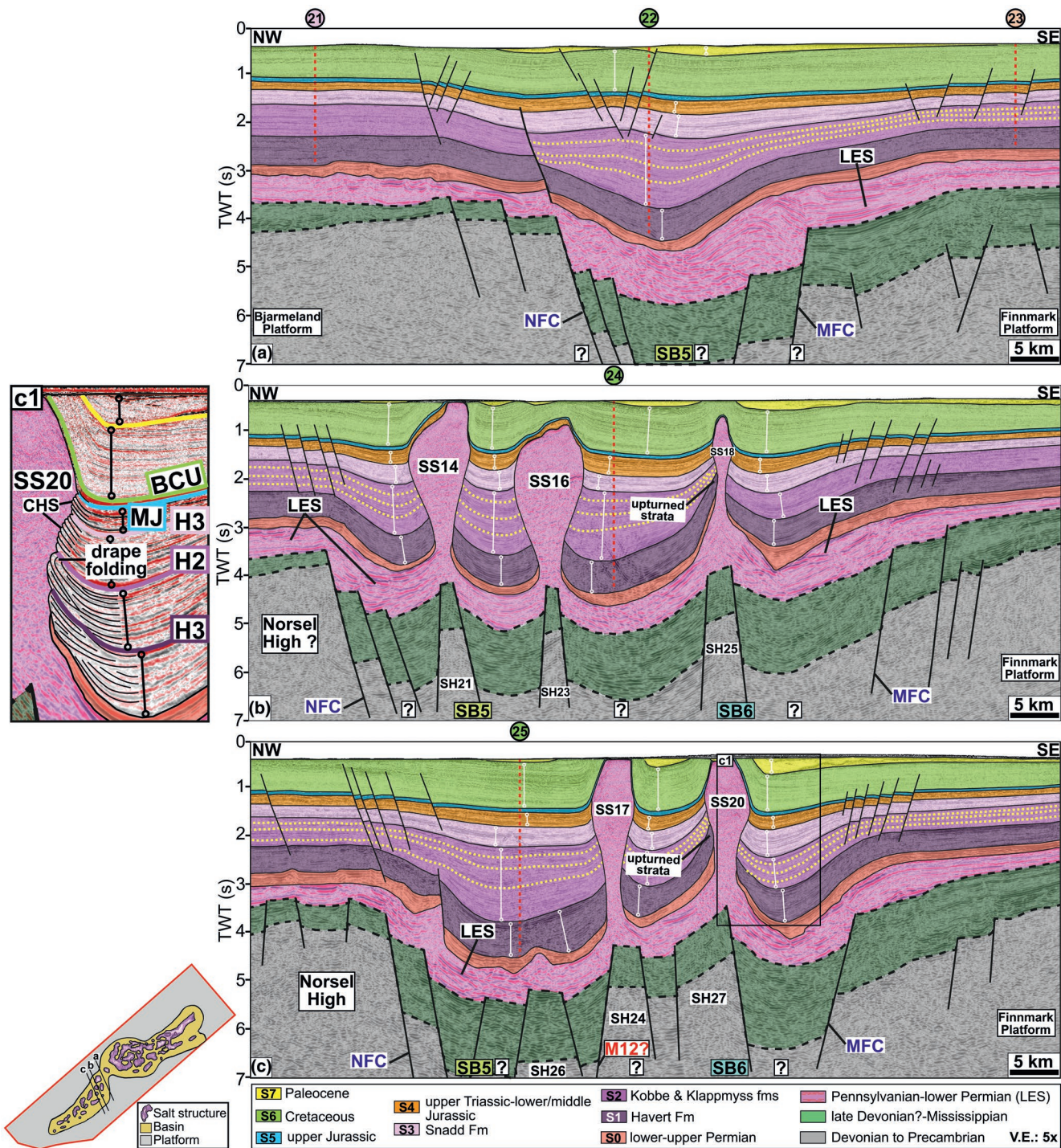
FIGURE 9 (a–d) Interpreted seismic sections (TWT, two-way travel time, s; vertical exaggeration: 5×) illustrating pre-evaporite geometries, layered evaporite sequence (LES), salt structures and post-salt sedimentation patterns in the central (CNB) Nordkapp Basin segment. (d1-2) Un-flattened and flattened seismic sections display internal architecture of a dwarf secondary mini-basin over the segment DFa. DF, Dragon foot; M, Master fault; SB, Sub-basin; SH, Structural high; TIFC, Thor Iversen Fault Complex. Colour-rasters correspond to interpreted sequences in Figure 2. Open white circles connected by white lines display the thickness variations and salt structures (SS) as in Figure 3c. Numbers 11–15 denote the locations of 1D backstripping models that were used to calculate sediment accumulation rates as in Figure 6 and Table 5. Profile locations also in Figure 1b. Seismic data courtesy of NPD and TGS
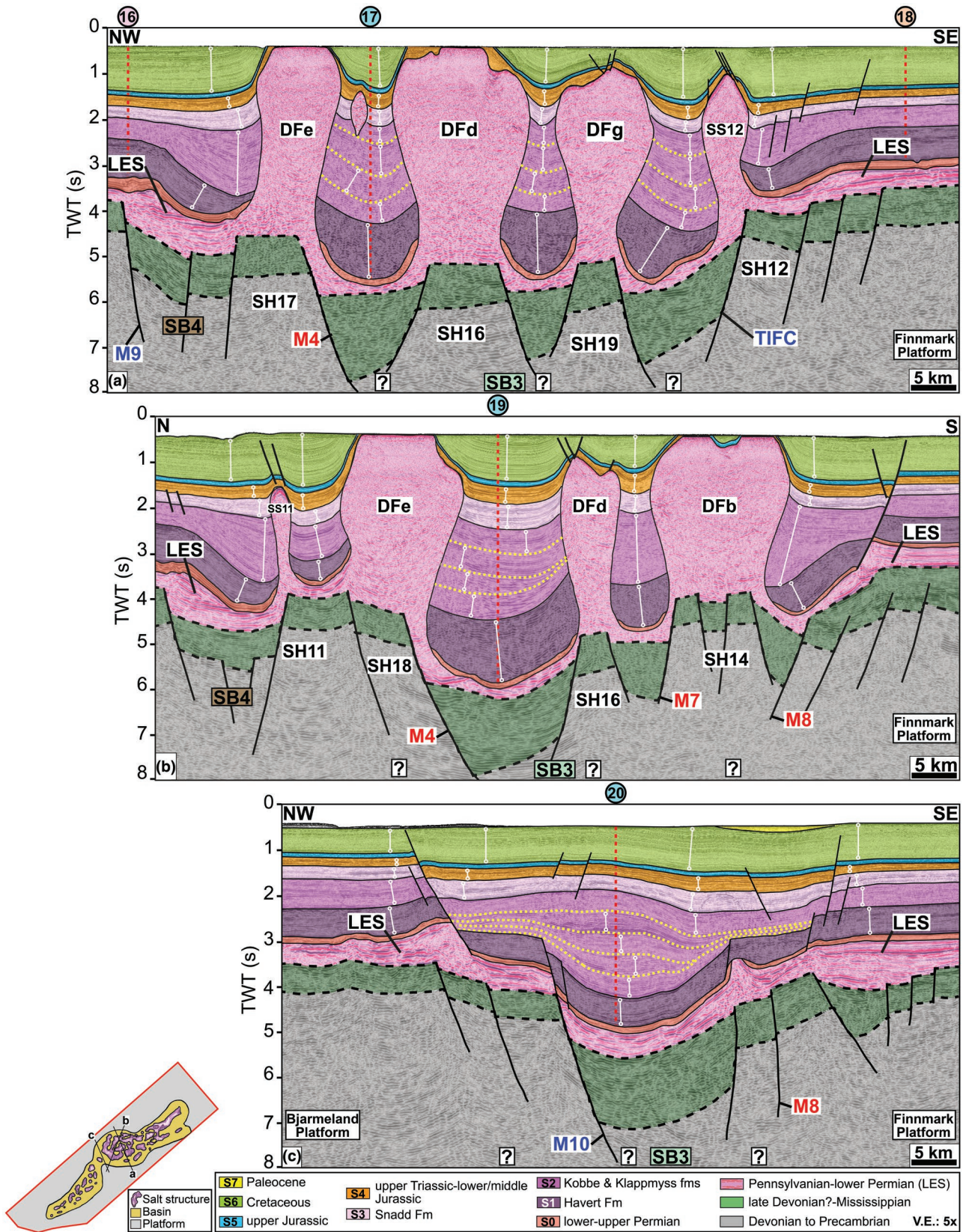
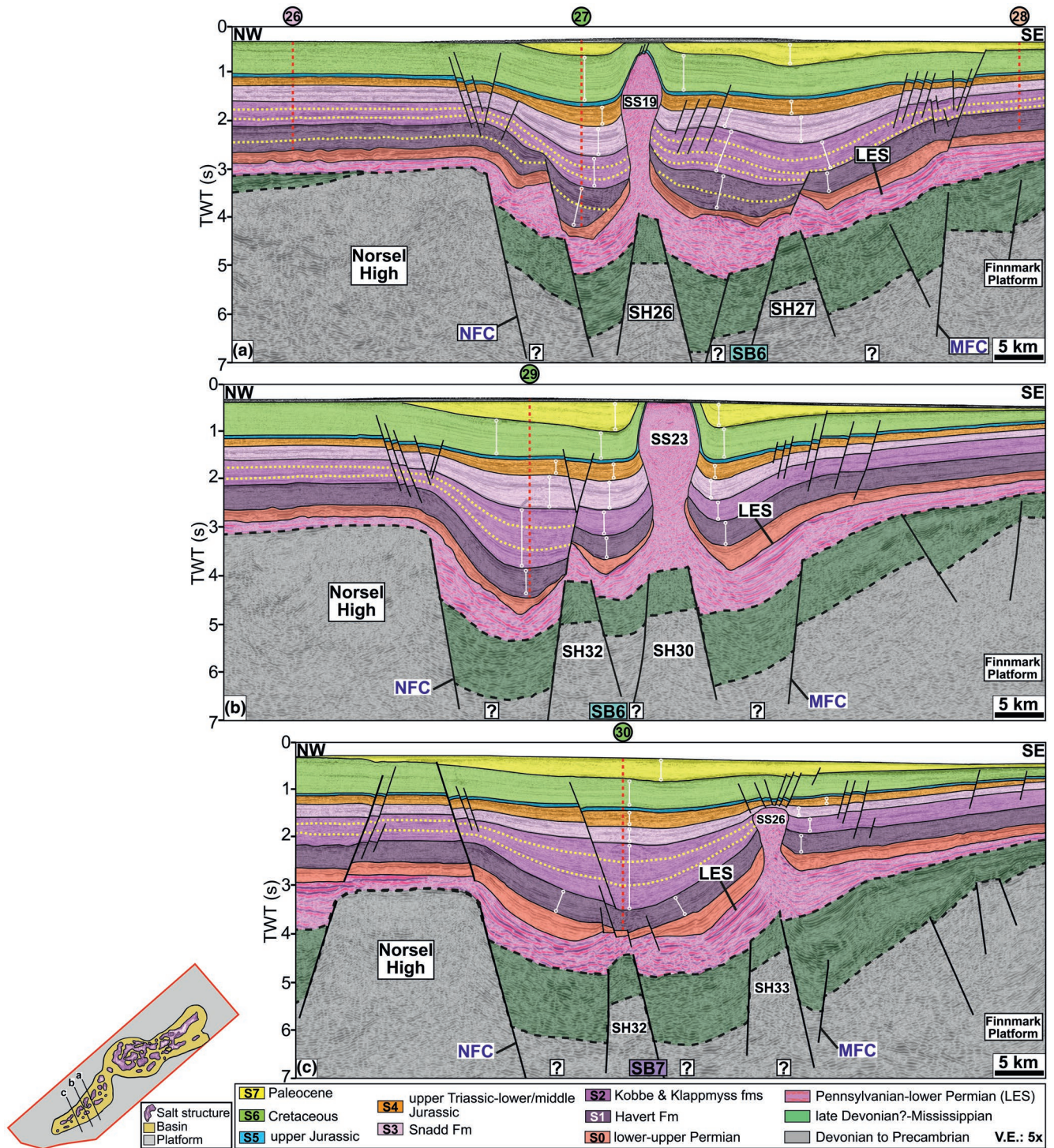**FIGURE 10** (a–c) Interpreted seismic sections (TWT, two-way travel time, s; vertical exaggeration: 5×) illustrating pre-evaporite geometries, layered evaporite sequence (LES), salt structures and post-salt sedimentation patterns in the central (CNB) Nordkapp Basin segment. DF, Dragon foot; M, Master fault; SB, Sub-basin; SH, Structural high; TIFC, Thor Iversen Fault Complex. Colour-rasters correspond to interpreted sequences in Figure 2. Open white circles connected by white lines display the thickness variations and salt structures (SS) as in Figure 3c. Numbers 16–20 denote the locations of 1D backstripping models that were used to calculate sediment accumulation rates as in Figure 6 and Table 5. Profile locations also in Figure 1b. Seismic data courtesy of NPD and TGS

FIGURE 11 (a–c) Interpreted seismic sections (TWT, two-way travel time, s; vertical exaggeration: 5×) illustrating pre-evaporite geometries, layered evaporite sequence (LES), salt structures and post-salt sedimentation patterns in the southwestern (SWNB) Nordkapp Basin segment. MFC, Måsoy Fault Complex; NFC, Nysleppen Fault Complex; SB, Sub-basin; SH, Structural high. Colour-rasters correspond to interpreted sequences in Figure 2. Open white circles connected by white lines display the thickness variations and salt structures (SS) as in Figure 3c. Numbers 21–25 denote the locations of 1D backstripping models that were used to calculate sediment accumulation rates as in Figure 6 and Table 5. Profile locations also in Figure 1b. Seismic data courtesy of NPD and TGS

map of sequence S2 displays abrupt thickness variations around the salt structures in comparison with the regional prograding sediment thickness (Figure 5b).

In the NENB segment, the seismic observations and the time-thickness map demonstrate that the depocenter of sequence S2 migrated to the NNW with time

FIGURE 12 (a–c) Interpreted seismic sections (TWT, two-way travel time, s; vertical exaggeration: 5×) illustrating pre-evaporite geometries, layered evaporite sequence (LES), salt structures and post-salt sedimentation patterns in the southwestern (SWNB) Nordkapp Basin segment. MFC, Måsøy Fault Complex; NFC, Nysleppen Fault Complex; SB, Sub-basin; SH, Structural high. Colour-rasters correspond to interpreted sequences in Figure 2. Open white circles connected by white lines display the thickness variations and salt structures (SS) as in Figure 3c. Numbers 26–30 denote the locations of 1D backstripping model that were used to calculate sediment accumulation rates as in Figure 6 and Table 5. Profile locations also in Figure 1b. Seismic data courtesy of NPD and TGS

(Figures 5b and 7a). The sediment accumulation rates at the Bjarmeland Platform are slightly higher (ca. 171–181 m/Myr) than the Finnmark Platform (ca. 146–152 m/Myr), whereas in the NENB segment the rates increase from NE (ca. 223 m/Myr) to SW (ca. 424 m/Myr) (Table 5a). The internal reflections in sequence S2 display

isopachous geometry across the Finnmark Platform and are affected by the NNW-dipping post-salt fault over the SH2 structural high (Figure 7a). Sequence S2 increases gradually in thickness towards NW with progressive shifting of depocenters, whereas its thickness is uniform across the Veslekari Dome (Figure 7a). Towards farther SW within sub-basin SB1, sequence S2 thickens drastically over the limb of the turtle structure to the southern flank of the SS1 salt wall in contrast to the northern flank (Figure 7b). However, dramatically thicker sediments of sequence S2 were accumulated asymmetrically towards NNW in contrast to the south-southeast side of the SS1 salt wall in vicinity of the turtle structure to SW (Figure 7b,c). Within sub-basin SB2, sequence S2 is thickening towards southeast in the collided mini-basin between the secondary welds, and farther SW between the SS4 and SS5 salt stock (Figure 8b,c).

Adjacent to the CNB segment, the sediment accumulation rates of sequence S2 on the Finnmark (ca. 163–173 m/Myr) and Bjarmeland (ca. 171–174 m/Myr) platforms are almost similar. However, in the CNB segment the rates are relatively lower in the NE (ca. 411 m/Myr) compared with the SW (ca. 504 m/Myr) (Figures 5b and 6b; Table 5b). Reflections within sequence S2 display tabular geometry over the Finnmark and Bjarmeland platforms, whereas the sequence becomes thicker near the salt structures in the CNB segment (Figures 9a,b and 10b,c). Within sub-basin SB3 sequence S2 thickens to the south-southeast along with the rotation (around a horizontal axis) of earlier formed mini-basin and development of salt wing to the segment DFg (Figure 9b). Internally, the wedge-shaped and tabular geometries are evident, and in some cases, the sequence S2 displays thickening in the opposite direction in comparison with the earlier deposited sequence S1 (Figure 9b,b2). The salt wing is ca. 3 km wide and ca. 5.5 km long, and is formed on the southeastern side of segment DFg and strikes NE-SW with SE dip (Figures 3c and 9b). Sequence S2 is thickest in the mini-basin along the DFb salt segment where internally the stacked growth sequences are slightly migrating towards NW (Figure 10c). In the outlier sub-basin SB4, sequence S2 thickens and onlaps both the salt walls DFe and SS11 (Figure 10a,b).

Within the SWNB segment, the sediment accumulation rates (ca. 349–381 m/Myr) are decreasing from the NE to SW. The rates on the adjacent Finnmark (ca. 141–171 m/Myr) and Bjarmeland (ca. 202 m/Myr) platforms, and Norsel High (ca. 165 m/Myr) show a similar trend (Figures 5b and 6b; Table 5c). The internal sequence S2 reflections on the Norsel High, and Finnmark and Bjarmeland platforms show isopachous geometry where mostly post-salt faults and occasionally the thick-skinned Nysleppen Fault Complex offset the strata at the basin margin (Figures 11 and 12). In the northeasternmost

depocenter of sub-basin SB5, sequence S2 displays similar thickness variations and growth successions as within sub-basin SB3 (Figures 10c and 11a). In sub-basin SB6, the sequence S2 thins and upturns along the flanks of salt stock SS18 and salt wall SS20 (Figure 11b,c). In addition, sequence S2 onlaps sequence S1 over the expulsion rollover structure that developed on the southeastern side of the SS19 salt wall (Figure 12a). Overall, depocenters containing thick successions of sequence S2 have been developed towards the Norsel High (Figures 11c and 12b,c).

4.2.4 | Upper Triassic (sequence S3)

The upper Triassic sequence S3 consists of successions belonging to the Snadd Formation (Ladinian to early Carnian) and thickens regionally from the southeast (ca. 100 ms twt) to NW (ca. 700 ms twt) (Figures 2 and 5c). In the different Nordkapp Basin segments, sequence S3 displays distinct thickness variations along the margins of salt structures in contrast to the platform regions, and the sequence generally thickens in the opposite fashion from NE to SW (Figures 5c and 6c).

In the NENB segment, a prominent depocenter with thick growth strata was developed between the northeastern edge of salt wall SS1 and the Veslekari Dome. The sediment accumulation rates of sequence S3 are higher within segment NENB (ca. 24–37 m/Myr) in contrast to the Finnmark (ca. 18–27 m/Myr) and Bjarmeland (ca. 22–25 m/Myr) platforms adjacent to it (Figure 5c; Table 5a). Within sequence S3, parallel seismic reflections show tabular geometry over the Finnmark and Bjarmeland platforms. In addition, within the NENB mini-basins, sequence S3 displays parallel reflections and thins near the salt structures (Figures 5c, 6 and 7).

The sediment accumulation rates in the CNB segment are higher (ca. 31–51 m/Myr) than in the Finnmark (ca. 25–26 m/Myr) and Bjarmeland platforms (ca. 28–30 m/Myr) adjacent to it (Figure 6b; Table 5b). Sequence S3 shows isopachous geometry on the platforms and is offset by the post-salt marginal faults when it enters the basin (Figures 9 and 10). Within the CNB segment, sequence S3 comprises parallel seismic reflections and its thickness is variable in the different mini-basins. Sequence S3 thins and onlaps the salt structures and occasionally sub-crops at the seafloor (Figures 9 and 10). Farther SW of the CNB segment, sequence S3 thickens towards the margins and thinning against the crest of the turtle anticline at the mini-basin axis, which was developed between segment DFb and the SS13 salt stock (Figure 10c). Sequence S3 exhibits higher sediment accumulation rates (ca. 38–57 m/Myr) in the SWNB segment than the NENB and CNB

TABLE 5 Calculated paleo-thicknesses and sediment accumulation rates based on 1D backstripping at specific locations (1–30) as in Figures 6–12 in the different segments (NENB, CNB and SWNB) of the Nordkapp Basin, as well as on the Finnmark (FP) and Bjarmeland (BP) platforms

(a) Northeastern Nordkapp Basin segment (NENB), Bjarmeland (BP) and Finnmark (FP) platforms

Sequence	1 (BP) Paleo-thickness m	1 (BP) Rate m/Myr	2 (NENB) Paleo-thickness m	2 (NENB) Rate m/Myr	3 (FP) Paleo-thickness m	3 (FP) Rate m/Myr	4 (NENB) Paleo-thickness m	4 (NENB) Rate m/Myr	5 (NENB) Paleo-thickness m	5 (NENB) Rate m/Myr	6 (BP) Paleo-thickness m	6 (BP) Rate m/Myr	7 (NENB) Paleo-thickness m	7 (NENB) Rate m/Myr	8 (FP) Paleo-thickness m	8 (FP) Rate m/Myr	9 (NENB) Paleo-thickness m	9 (NENB) Rate m/Myr	10 (NENB) Paleo-thickness m	10 (NENB) Rate m/Myr
Sequence S5	209	12	231	11	208	10	261	13	253	3	274	14	234	12	232	12	242	12	273	14
Sequence S4	326	7	356	6.5	251	5	298	6	393	8	286	6	513	10	372	7	558	11	602	12
Sequence S3	585	24	638	22	483	18	709	27	735	28	651	25	874	33	725	27	899	34	978	37
Sequence S2	1,416	330	2,742	171	1,261	152	1,853	223	1,747	211	1,505	181	2,455	296	1,210	146	2,650	319	3,520	424
Sequence S1	2,140	1,366	2,869	1,019	2,310	1,100	3,866	1,841	5,372	2,558	2,407	1,146	5,436	2,589	2,294	1,092	5,206	2,479	4,067	1,937

(b) Central Nordkapp Basin segment (CNB), Bjarmeland (BP) and Finnmark (FP) platforms

Sequence	11 (BP) Paleo-thickness m	11 (BP) Rate m/Myr	12 (CNB) Paleo-thickness m	12 (CNB) Rate m/Myr	13 (FP) Paleo-thickness m	13 (FP) Rate m/Myr	14 (CNB) Paleo-thickness m	14 (CNB) Rate m/Myr	15 (CNB) Paleo-thickness m	15 (CNB) Rate m/Myr	16 (BP) Paleo-thickness m	16 (BP) Rate m/Myr	17 (CNB) Paleo-thickness m	17 (CNB) Rate m/Myr	18 (FP) Paleo-thickness m	18 (FP) Rate m/Myr	19 (CNB) Paleo-thickness m	19 (CNB) Rate m/Myr	20 (CNB) Paleo-thickness m	20 (CNB) Rate m/Myr
Sequence S5	289	15	345	17	213	11	400	20	349	18	328	16	313	16	271	14	373	19	279	14
Sequence S4	413	8	564	11	393	8	531	11	635	13	424	9	567	11	353	7	669	13	448	9
Sequence S3	734	28	1,112	42	693	26	821	31	849	32	795	30	1,042	39	671	25	1,352	51	937	35
Sequence S2	1,440	174	3,554	428	1,438	173	3,415	411	3,824	461	142	171	4,046	488	1,351	163	3,868	466	4,183	504
Sequence S1	2,407	1,146	4,425	2,107	2,362	1,125	5,541	2,639	3,382	1,611	2,482	1,182	3,690	1,757	2,221	1,058	4,026	1,917	2,444	1,164

(c) Southwestern Nordkapp Basin segment (SWNB), Norsel High (NH), Bjarmeland (BP) and Finnmark (FP) platforms

Sequence	21 (BP) Paleo-thickness m	21 (BP) Rate m/Myr	22 (SWNB) Paleo-thickness m	22 (SWNB) Rate m/Myr	23 (FP) Paleo-thickness m	23 (FP) Rate m/Myr	24 (SWNB) Paleo-thickness m	24 (SWNB) Rate m/Myr	25 (SWNB) Paleo-thickness m	25 (SWNB) Rate m/Myr	26 (NH) Paleo-thickness m	26 (NH) Rate m/Myr	27 (SWNB) Paleo-thickness m	27 (SWNB) Rate m/Myr	28 (FP) Paleo-thickness m	28 (FP) Rate m/Myr	29 (SWNB) Paleo-thickness m	29 (SWNB) Rate m/Myr	30 (SWNB) Paleo-thickness m	30 (SWNB) Rate m/Myr
Sequence S5	257	16	310	13	231	12	286	14	257	13	190	10	289	15	188	9	268	13	237	12
Sequence S4	354	10	491	7	356	7	700	14	575	12	354	7	746	15	291	6	599	12	619	12
Sequence S3	796	44	1,159	30	707	27	1,016	38	1,092	41	855	32	1,463	55	608	23	1,505	57	997	38
Sequence S2	1,677	381	3,160	202	1,419	171	3,055	368	3,151	380	1,367	165	1,981	239	1,174	141	2,835	342	2,895	349
Sequence S1	2,002	1,169	2,455	953	1,664	792	2,467	1,175	2,614	1,245	1,843	878	2,521	1,201	1,572	749	2,441	1,162	2,098	999

segments (Figure 6b; Table 5c). In addition, sequence S3 shows sub-parallel seismic reflections and isopachous stacked geometry over the Finnmark and Bjarmeland platforms. Gradually, sequence S3 becomes thicker in the mini-basins and onlaps the salt structures in contrast to the tabular strata on the Finnmark and Bjarmeland platforms. In particular, sequence S3 displays asymmetric deposition and thins towards the SS20 salt wall due to the development of the upturned strata (Figure 11b,c). Clear thinning of sequence S3 can be observed above the SS26 salt stock that never pierced through the upper Triassic to Cenozoic strata (Figure 12c).

4.2.5 | Upper Triassic-lower/middle Jurassic (sequence S4) to upper Jurassic (sequence S5)

Sequences S4 and S5 comprise siliciclastic successions of the Fruholmen, Tubåen, Nordmela, Stø, Fuglen and Hekkingen formations (Figure 2). The combined regional thickness map for the sequences display an NW increase reaching ca. 300 ms twt thickness. Individually, the low sediment accumulation rates of sequences S4 (ca. 6–15 m/Myr) and S5 (ca. 10–20 m/Myr) contrast the ones for sequences S1–S3 (Figures 5d and 6d,e; Table 5). The sediment accumulation rate curve for sequence S4 follows the same trend as sequence S3 and increases to the SW within the Nordkapp Basin (Figure 6).

In the NENB segment, a depocenter of sequence S4 was formed between the northeastern edge of the SS1 salt wall and the Veslekari Dome. Minor thickness variations can be observed around the SS2 salt wall and in the depocenter that was formed between the SS1 and SS3 salt walls (Figures 5d and 7a,b). Sequence S4 is characterized by parallel reflections, it shows tabular geometry on the Finnmark and Bjarmeland platforms and is offset by the post-salt marginal faults. Furthermore, sequence S4 is upturned along the flanks of the salt structures and sub-crops at the seafloor (Figures 7 and 8). In particular within sub-basin SB2, the southeastern side of the collided mini-basin is pushed up due to the thick-skinned reverse fault (Figure 8b, red arrow) where a thin S4 sequence sub-crops at the seafloor.

In the CNB segment, sequence S4 thickens within the mini-basins in contrast to the Finnmark and Bjarmeland platforms where it displays tabular geometry (Figures 9 and 10). Most of the lower successions of sequence S4 onlap the salt structures, whereas the upper successions of the sequence are upturned along their flanks and sub-crop at the seafloor. A dwarf secondary mini-basin (sensu Jackson & Hudec, 2017) was developed over the DFa segment where the mini-basin is tilted towards the east. The western part of

the dwarf secondary mini-basin together with the salt wall sub-crop at the seafloor (Figure 9d). It is noteworthy that sequence S4 shows thickness variations within the partially eroded dwarf secondary mini-basin above segment DFa (Figure 9d). In the SWNB segment, sequence S4 thickens in the mini-basins and onlaps the salt structures (Figures 11 and 12). In the same segment, sequence S5 comprises highly condensed successions that are upturned along the flanks of the salt structures and sub-crop at the seafloor.

4.2.6 | Cretaceous (sequence S6) to Cenozoic (sequence S7)

Sequences S6 and S7 comprise the Lower Cretaceous Knurr, Klippfisk, Kolje and Kolmule formations and Cenozoic strata (Figure 2). Sequence S6 displays parallel and inclined seismic reflections on the Finnmark and Bjarmeland Platforms, and on the Norsel High. Within the Nordkapp Basin, sequence S6 shows considerable thickness in the mini-basins, whereas the seismic reflections are upturned along the flanks of the salt structures and sub-crop at the seafloor (Figures 7–12). Regionally, sequence S6 thins from the NE to the SW. Finally, although the entire sequence S7 is missing in the NENB and CNB segments a considerably thick Cenozoic (Paleocene) sequence S7 can be observed in the SWNB segment where it is upturned along with sequence S6 and both sub-crop at the seafloor (Figures 11 and 12).

4.3 | Structural restoration

To investigate the temporal evolution of the Nordkapp Basin, 2D structural restoration of the selected depth-converted seismic sections was performed in time-steps corresponding to the ages of the interpreted horizons. We considered mobile and non-mobile LES as a single layer for modelling purposes. The residual LES at the present-day stage of all models correspond to non-mobile evaporites in the Nordkapp Basin (Figures 13–16).

4.3.1 | Pennsylvanian to late Permian

The Pennsylvanian to early Permian LES (Gipsdalen Group, Figure 2) was accumulated during syn-rift to early post-rift conditions, and the LES sediment facies and deposition were influenced by the basement faults, structural highs and half-graben architecture (Figure 3b; Hassaan et al., 2021b). Within the different segments of the Nordkapp Basin, the sub-basins were further subdivided by the structural highs that later localised the

salt structures and post-salt depocenters (Figures 13A1–B1, 14A1, 15A1–B1, and 16A1–B1). During the early to late Permian, carbonate-dominated successions of the Bjarmeland and Tempelfjorden groups (sequence S0; Figure 2) were deposited in the Nordkapp Basin and in the platform regions. The restored thickness of sequence S0 seems to be uniform over the LES in the NENB and in the northeastern part of the CNB segments but influenced by the minor faulting caused by the mid-late Permian regional extension (Figures 13A1–B1, 14A1, and 15A1–B1). Within the SWNB and southwestern part of the CNB segments, sequence S0 thins to a minimum above inflated salt over the structural highs, whereas it thickens in the depocenters surrounding it that are partially controlled by minor normal faulting caused by the mid-late Permian regional extension (Figures 4b and 16A1–B1). The minor faulting and salt mobilisation developed residual topography that mimics the pre-salt rift architecture and created preferential sediment deposition locations for the later prograded sediments in the Nordkapp Basin. Slight local thickness variation of sequence S0 is also visible over the Finnmark and Bjarmeland platforms (Figures 13A1–B1 and 14A1–B1).

4.3.2 | Earliest Triassic

In the NENB segment, the mini-basins were filled with successions of the lower Triassic fluvio-deltaic sequence S1 (Havert Formation; Figure 2), which prograded from the east, and this caused progressively salt expulsion to the NNW (Figures 13A1–B1 and 14A2–A7). Sequence S1 can be sub-divided into three units, the lower, middle and upper, within the NENB segment. The lower unit seems to be influenced by the base-salt structural relief and the salt pillow formation over the SH1 structural high (Figure 14A2). The thick middle unit consists of several growth packages in the southern mini-basin that progressively led to depletion of the LES underneath. The growth packages onlap the lower unit that is upturned along the flank of the rising SS1 salt wall (Figure 14A3–A7). It is noteworthy that the depositional thickness of sequence S1 is comparatively less in the northern mini-basin. The upper unit thins gradually towards the SS1 salt wall and thickens to the south over the salt pillow as salt initiated to deplete from it and probably moved towards the adjacent SS2 salt wall (Figures 7b,c and 14A7–A8). Farther SW in the NENB segment, two narrow salt stocks that were formed over the fault structurally blocks have affected the development of the mini-basins (Figure 13B2). It seems that the salt structures were nucleated above the intra-basinal highs whereas the minor mid-late Permian normal faulting was amplified by the

accelerated sediment accumulation and loading. In the northeastern part of the CNB segment, sequence S1 filled the mini-basin between the SS8 salt stock and segment DFg in a similar fashion as the southern mini-basin of the SS1 salt wall was progressively filled (Figures 14A7 and 15A2). Eventually, the thickness of sequence S1 gradually decreases farther SW in the CNB and SWNB segments (Figure 16A1–B1).

4.3.3 | Early-mid-Triassic

In the NENB segment, growth strata of the prograding sequence S2 onlap sequence S1 over the salt pillow and form the NNW migrating depocenters. The asymmetric depocenter is rotated (around a horizontal axis) and tilted to the northwards due to the progressive salt expulsion from the earlier pillow structure in the SB1 sub-basin (Figure 13A3). The restoration illustrates that the SS1 salt wall was mainly sourced by salt evacuated from beneath the northern mini-basin, and the longest depocenter was formed due to this salt depletion (Figures 5b and 14A9–A11). At the same time, the depocenter also shifted to the south as the salt started to deplete from the salt anticline and moved into the SS2 salt wall (Figures 7b,c and 14A9–A11). Farther SW in the SB2 sub-basin, sequence S2 thickens to the south between the two narrow salt structures and is rotated (around a horizontal axis) and tilted to the southeast together with sequence S1 underneath it (Figure 13B2–B3). It seems that the increase in thickness of sequence S2 is also facilitated by the pre-salt fault-block arrangement in the structurally highly active region due to transfer zone (Figure 13B1). In the northeastern part of the CNB segment (SB3 sub-basin), the internal successions of sequence S1 in the mini-basin between the SS8 salt stock and segment DFg are rotated (around a horizontal axis) due to the shift in salt withdrawal and the thickening of sequence S2 towards the south (Figure 15A3). This intense salt evacuation and the rotation of the mini-basins facilitated the development of the salt wing on the southern flank of the DFg segment (Figure 15A3). Overall, the thickness of sequence S2 is increasing towards the SW within the CNB segment (Figure 8b). In the SWNB segment, the thickest depocenters formed towards the Norsel High and the evacuated mobile salt beneath them moved into the adjacent salt structures. During this time, the upturned strata started to develop due to the asymmetric salt evacuation caused by the prograding sequence S2 (Figures 11b,c and 16A3).

4.3.4 | Late Triassic to mid-Jurassic

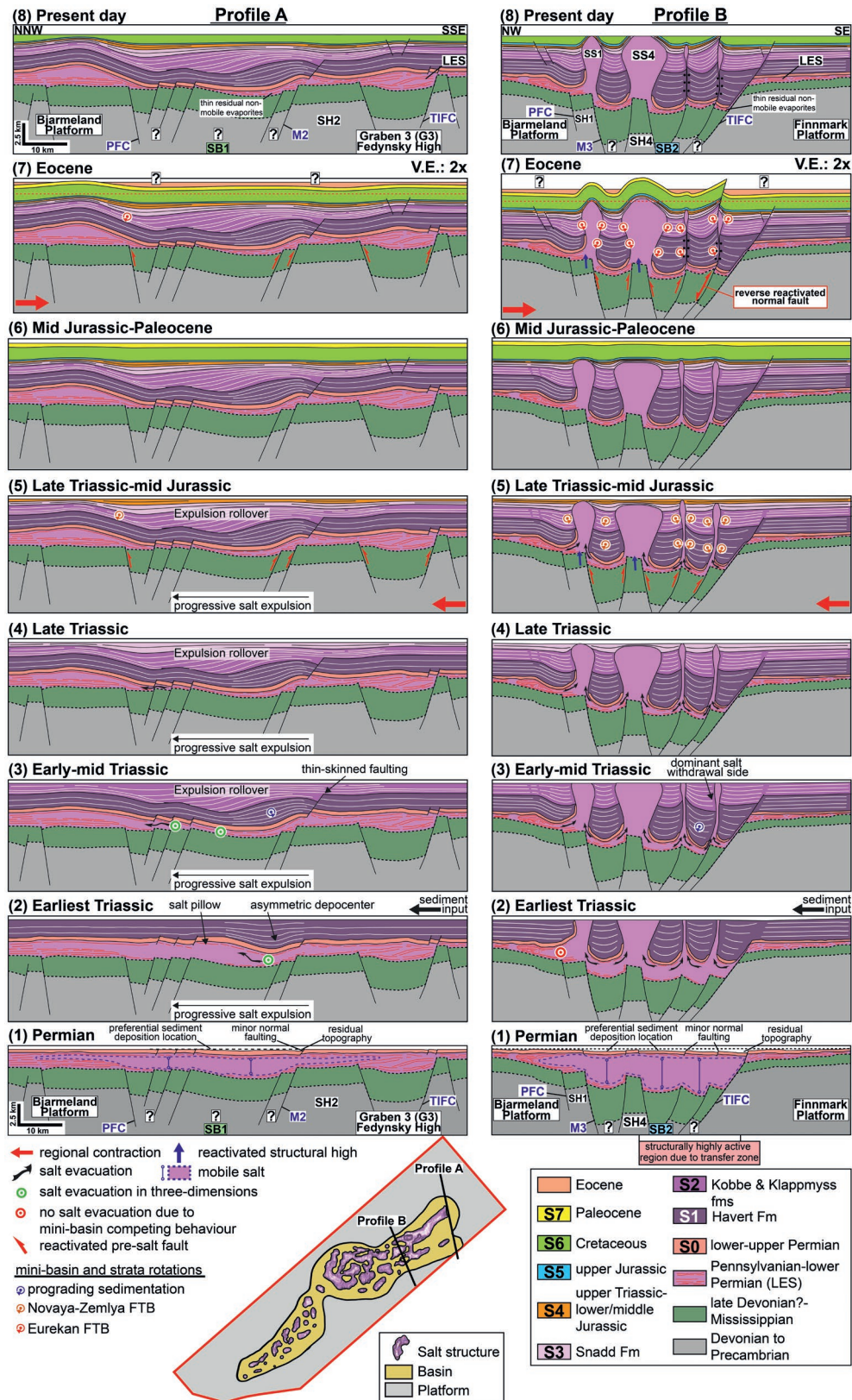Within the NENB segment, the migrating depocenters were developed at the southern edge of the Veslekari Dome
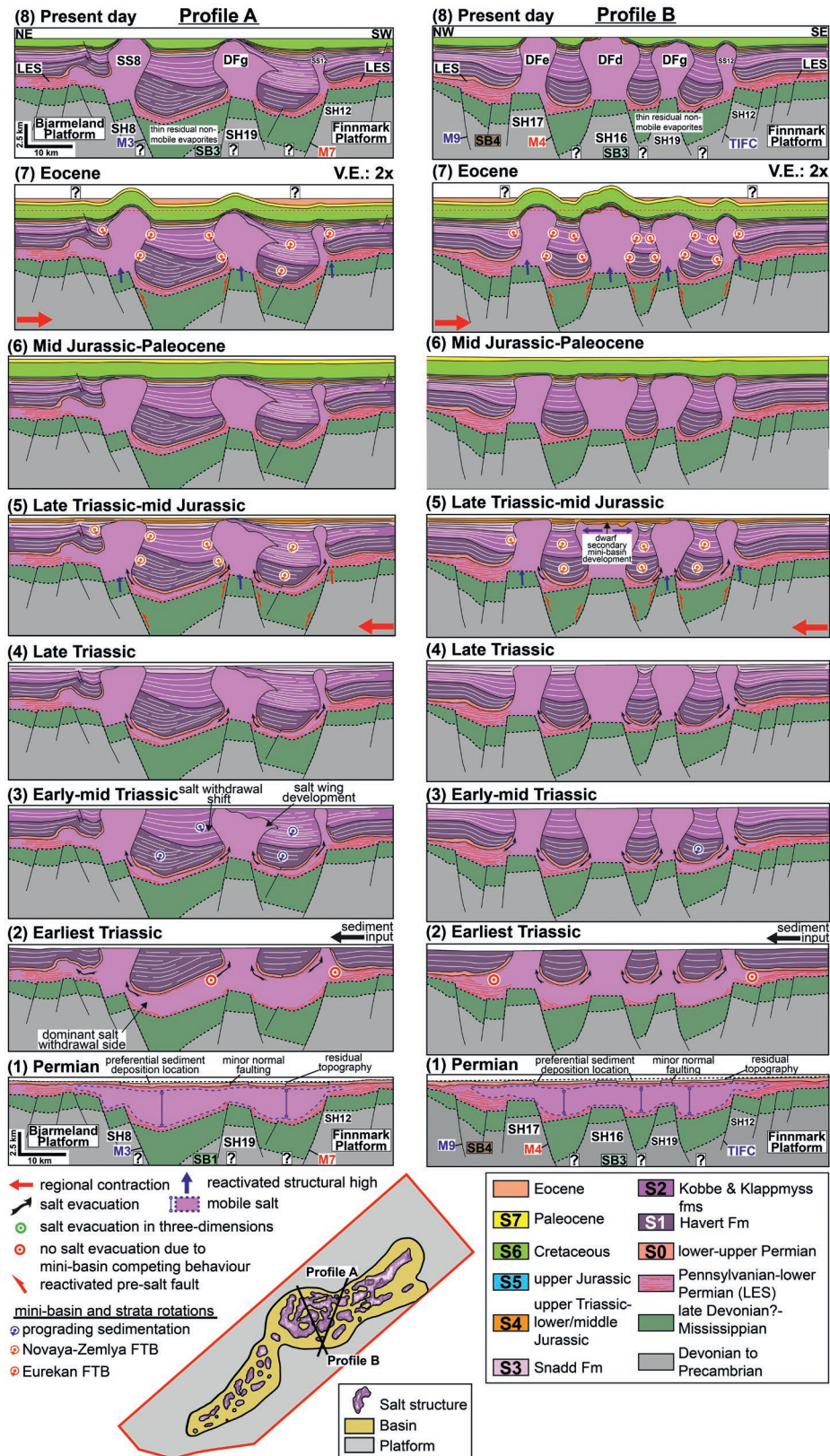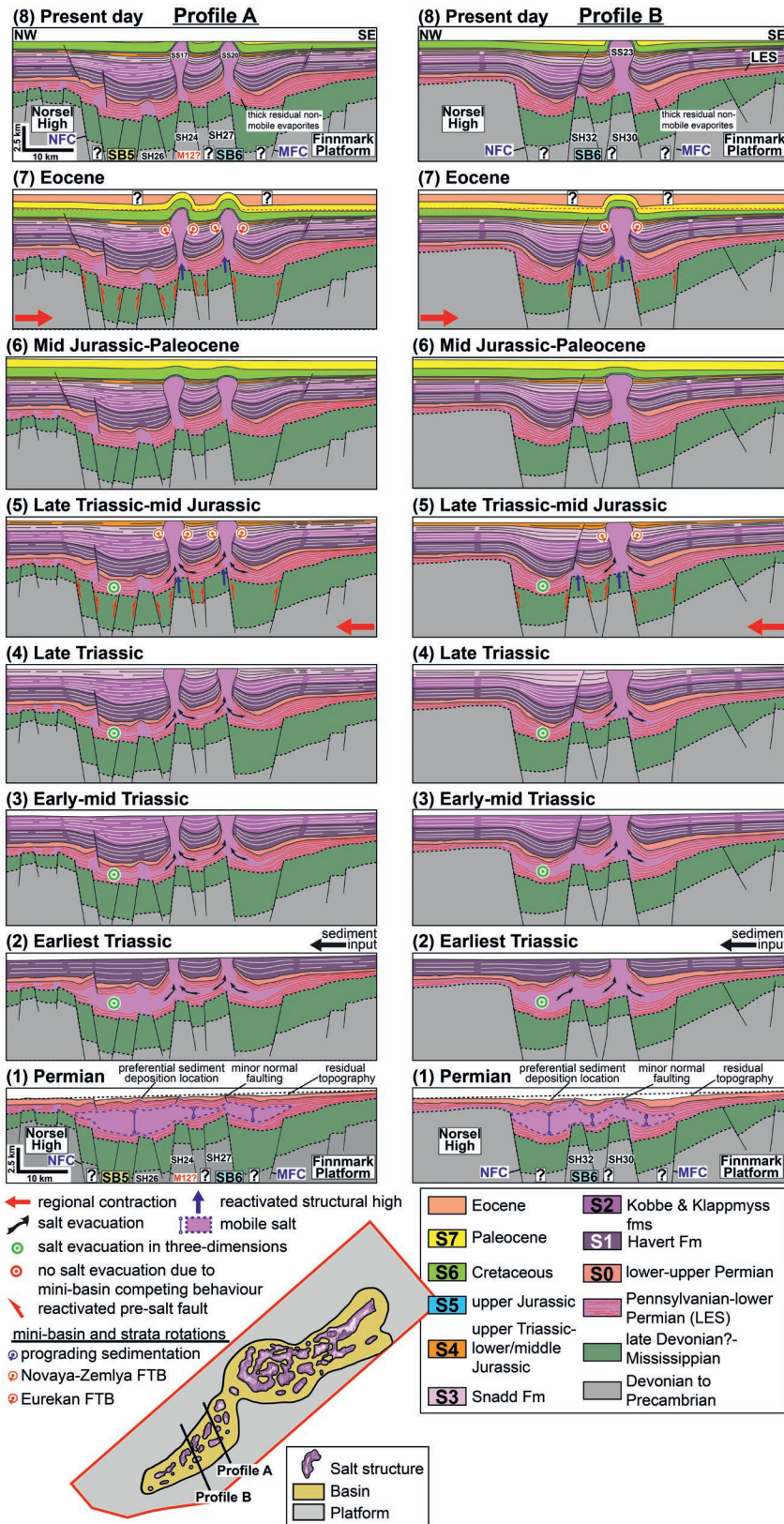
FIGURE 13 Sequential structural restoration of the interpreted and depth-converted sections (vertical exaggeration: 2×) Profile A (Figure 7a) and Profile B (Figure 8b) showing the post-salt evolution of the northeastern (NENB) Nordkapp Basin segment. The models display the salt flow direction (within and out of plane or three dimensions), influence of the far-field stresses during the Triassic–Jurassic transition and early-mid Eocene, and rotation of mini-basins. FTB, fold-and-thrust belt; LES, layered evaporite sequence; M, Master fault; PFC, Polstjerna Fault Complex; SB, Sub-basin; SH, Structural high; SS, Salt structure; TIFC, Thor Iversen Fault Complex. See the text for details and discussions. Inset map shows location of the sections as in Figure 1b
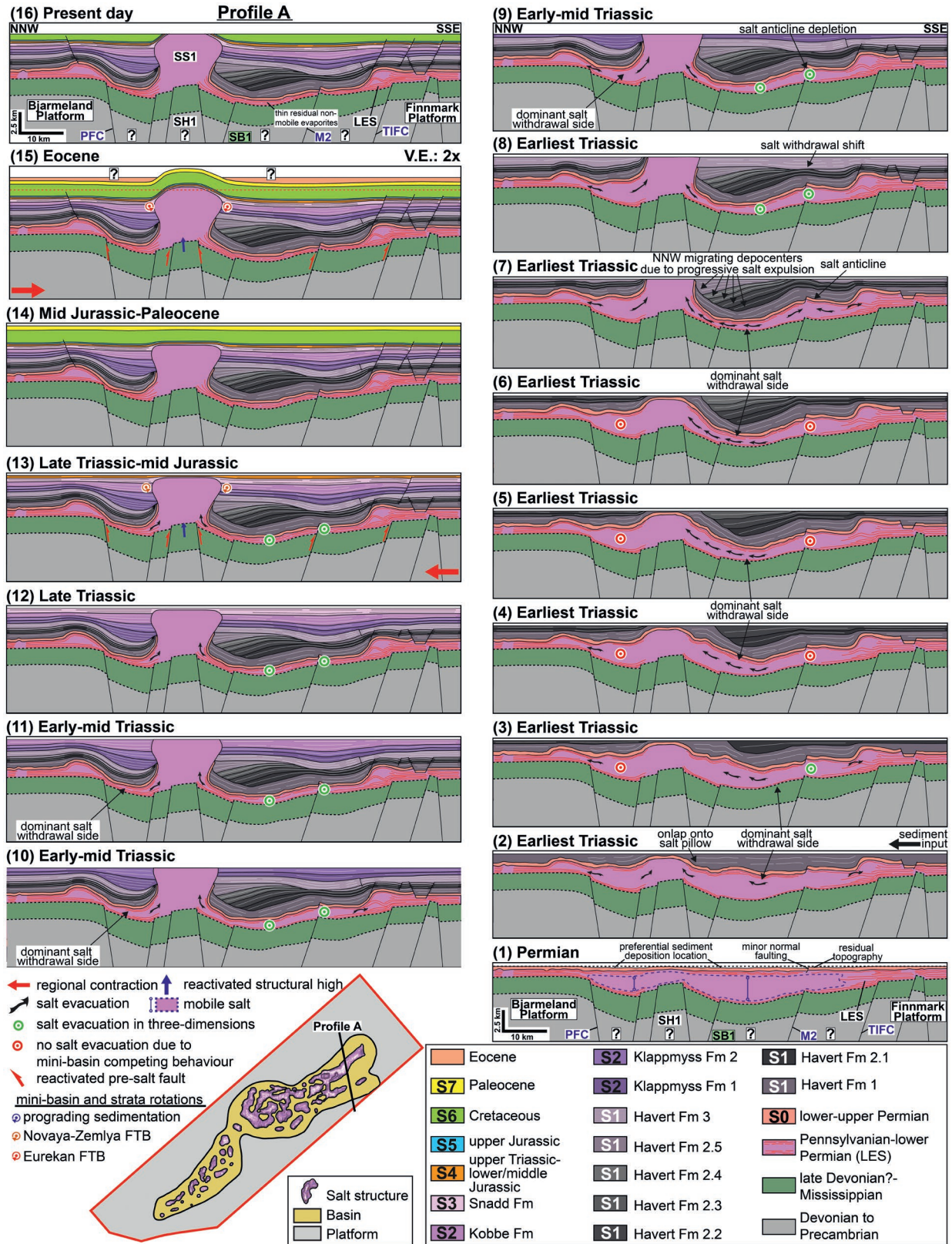
FIGURE 14 Sequential structural restoration of the interpreted and depth-converted section (vertical exaggeration: 2×) Profile A (Figure 7c) showing the post-salt evolution of the northeastern (NENB) Nordkapp Basin segment. The models shows the salt flow direction (within and out of plane or three dimensions), influence of the far-field stresses during the Triassic–Jurassic transition and early-mid Eocene, and rotation of mini-basins. FTB, fold-and-thrust belt; LES, layered evaporite sequence; M, Master fault; PFC, Polstjerna Fault Complex; SB, Sub-basin; SH, Structural high; SS, Salt structure; TIFC, Thor Iversen Fault Complex. See the text for details and discussions. Inset map shows the location of the section as in Figure 1b

FIGURE 15 Sequential structural restoration of the interpreted and depth-converted sections (vertical exaggeration: 2×) Profile A (Figure 9b) and Profile B (Figure 10a) showing the post-salt evolution of the central (CNB) Nordkapp Basin segment. The models display the salt flow direction (within and out of plane or three dimensions), influence of the far-field stresses during the Triassic–Jurassic transition and early-mid Eocene, and rotation of mini-basins. DF, Dragon foot; FTB, fold-and-thrust belt; LES, layered evaporite sequence; M, Master fault; SB, Sub-basin; SH, Structural high; SS, Salt structure; TIFC, Thor Iversen Fault Complex. See the text for details and discussions. Inset map shows the location of the sections as in Figure 1b

FIGURE 16 Sequential structural restoration of the interpreted and depth-converted sections (vertical exaggeration: 2×) Profile A (Figure 11c) and Profile B (Figure 12b) showing the post-salt evolution of the southwestern (SWNB) Nordkapp Basin segment. The models show the salt flow direction (within and out of plane or three dimensions), influence of the far-field stresses during the Triassic–Jurassic transition and early-mid Eocene, and rotation of mini-basins. FTB, fold-and-thrust belt; LES, layered evaporite sequence; MFC, Måsøy Fault Complex; NFC, Nysleppen Fault Complex; SB, Sub-basin; SH, Structural high; SS, Salt structure. See the text for details and discussions. Inset map shows the location of the sections as in Figure 1b

due to the NNW salt expulsion and the deposition of the prograding sediments (Figure 13A4–A5). Farther SW, the salt structures display significant growth but are eventually encompassed by thin strata that belong to sequences S3 and S4 forming composite halokinetic sequences (CHS) associated with the diapir downbuilding (Figure 14A12–A13) (sensu Giles & Rowan, 2012; Pichel & Jackson, 2020). In the CNB segment, the salt structures display downbuilding as sequence S3 thickens in the mini-basins and onlaps the flanks of the salt structures (Figure 15A4–A5, B4–B5).

A dwarf secondary mini-basin formed at the crest of segment DFd and was filled with successions of sequence S4 (Figure 15B5). The mini-basins around the DFg segment show the complex development as thick successions of sequences S3 and S4 onlap the northern flank of the segment, whereas within the southern mini-basin the same sequences thin and onlap the earlier deposited strata (Figure 15A4–A5). Within the SWNB segment, the thickest depocenters developed towards the Norsel High due to the significant salt evacuation from the LES as thick mobile salt was available in the deep ponds towards the structural high (Figure 16A4–A5, B4–B5). Occasionally due to the mini-basin development, sequences S3 and S4 were influenced by the thin-skinned faults and onlap the salt structures (Figure 16B4–B5). The upturned strata were further developed along with the SS20 salt wall, as it is evident by the asymmetric sediment deposition (Figure 16A4). Sequences S3 and S4 thin towards the northwestern flank, whereas thicken towards the southeastern flank of the SS20 salt wall (Figure 16A4–A5).

4.3.5 | Mid-Jurassic to present

During the mid-Jurassic to early Cretaceous, slight growth of the salt structures can be observed while condensed upper Jurassic successions are draped over them in the entire Nordkapp Basin. Regionally, the lower Cretaceous strata thin, whereas the Palaeocene strata become thicker towards the SW (Figures 13A7 and 16A7). Inside the Nordkapp Basin, however, these prograding sediments thicken in the mini-basins, but are relatively thin above the salt structures (Figures 13A6–B6, 14A14, 15A6–B6, and 16A6–B6). During the Eocene, the salt structures were rejuvenated by contractional deformation and the late Triassic to Palaeocene strata became upturned along the flanks (Figures 13A7–B7, 14A15, 15A7–B7, and 16A7–B7). At the same time, the Eocene sediments probably onlapped the rising Palaeocene strata due to the growth of the salt structures. However, re-distribution of eroded lower Cretaceous and Palaeocene sediments around the peripheral sinks cannot be ruled out. In the Neogene, due to uplift and erosion, approximately 1,500 m of strata were removed above the Nordkapp Basin (Figures 13A8–B8, 14A16, 15A8–B8, and 16A8–B8).

5 | DISCUSSION

5.1 | Pre-salt rift architecture and layered evaporite sequence distribution

The basement topography comprised the Timanian and Caledonian structures that facilitated the creation of the seven sub-basins SB1-7 during the late Devonian-early Carboniferous and late Carboniferous extensional phases in the Nordkapp Basin (Figure 4a; Hassaan et al., 2021b). The late Carboniferous-early Permian LES accumulation was influenced by the syn- to early post-rift processes, the internal configuration of the sub-basins as a result of cross-cutting master faults, and the arrays of structural highs (Figure 3b). However, not only the facies and the thickness of the LES influence by the pre-salt basin topography that vary from the margin to the deep basin, but so do the relative movement of the master faults and the architecture of the structural highs that have created the isolated ponds within the sub-basins (Figure 3b; Gabrielsen et al., 1992; Jensen & Sørensen, 1992; Clark et al., 1998; Jackson & Hudec, 2017; Jackson et al., 2018; Rodriguez et al., 2018; Rowan et al., 2019). Furthermore, the facies variations of the LES from mobile to non-mobile are dependent on the siliciclastic sediment input in the basin, mineralogy, fluid-supported mineral transformations and the depositional environment during the evaporite accumulation processes (Warren, 2016). For example, the paleo-hinged margin contains in average present-day thicker evacuated mobile salt (sub-basin SB1: ca. 2.3 km) than the deep graben (sub-basin SB5: ca. 1.6 km) of the Nordkapp Basin (Figure 3). However, the residual non-mobile LES is thicker in sub-basin SB5 than sub-basin SB1, probably due to the additional input of eroded siliciclastics from the Norsel High (Figures 7c and 11a; Hassaan et al., 2021b). We suggest that these discrepancies and lithological changes would also influence the later salt mobilisation and rate of salt structure rise.

The scattered structural highs and master faults acted as precursors for the localisation of the salt structures that influenced the post-salt sedimentation in the Nordkapp Basin (Figures 7–12). These salt structures were fed through multiple ponds filled with LES where deeper pond contained thicker mobile salt that controlled their along-strike structural development, that is, the DF salt structure (Figure 3; Hassaan et al., 2021b). The sub-basins with variable rift architecture and thick LES are likely to respond differently to the sediment loading compared with the platform areas (Figures 7–12). The downbuilding of the thick strata was promoted by the drastic salt evacuation from the isolated ponds filled with the LES (Figure 3). The thicker post-salt clastic successions are found within the axial zone of the rift or in locations of high extension that could contain the thicker LES and are indirectly reflected in the rift architecture (Rojo et al., 2019; Stewart et al., 1997; Withjack & Callaway, 2000). Conversely, the areas with thinner LES, that is, faulted basin margins and hinged-margins, may not have a drastic effect other than the decoupling of the deformation above and below the LES. Furthermore, the relative presence of mobile (i.e. halite) versus non-mobile (i.e. anhydrite and carbonate) lithologies within the thinner LES would also influence

the structural style at the margins. The formation of fault-related salt wedges and post-salt fault complexes would be promoted if the mobile salt contents are higher in contrast to non-mobile evaporite along the margins due to salt mobilisation (Figures 7 and 9a,b; Jackson & Hudec, 2017; Stewart, 2007). However, the observed structural styles are characterized by the lack of salt pillows and thick-skinned faults between the basement and post-salt strata at the localities where the LES is mainly dominated by non-mobile anhydrite and carbonate lithologies (Figures 8, 9c, 11a and 12c) (Rojo et al., 2019).

5.2 | Timing and triggering mechanisms for salt mobilisation

5.2.1 | Mid-late Permian extension

The post-salt sedimentation following LES accumulation was initiated with the deposition of the late Palaeozoic cold-water carbonates of the Bjarmeland and Tempelfjorden groups (Figure 2) in the Barents Sea (Larssen et al., 2002; Stemmerik, 2000). At the same time, a regional extension took place during the mid-late Permian and influenced the fault dynamics and subsidence in the southwestern Barents Sea (Blaich et al., 2017; Clark et al., 2014; Faleide et al., 1984, 2018; Tsikalas et al., 2021). We suggest that the deep Caledonian structures beneath the Nordkapp Basin were slightly reactivated due to the mid-late Permian extensional phase and caused minor fault activity at the base Carboniferous level (Figure 4). At the same time, the salt from the LES was slightly mobilised towards the structural highs, and relatively thick lower-upper Permian strata were accumulated in the mini-basins separated by minor normal faults in the SWNB segment (Figures 5b, 12c, and 16A1–B1). On the other hand, the regional extension seems to have less influenced the Timanian basement-structures underneath the Nordkapp Basin but caused minor normal faulting and thickness variations in the lower-upper Permian strata (Figure 5b). Minor salt evacuations in the platform regions appear to be localised and have created an overall pre-kinematic relation with the non-mobile LES (Figures 7–9; Rojo et al., 2019; Rowan & Lindsø, 2017). The basement-influenced extension had terminated within the Nordkapp Basin but the remnant topography caused by the minor normal faulting and salt mobilisation existed at the onset of the Triassic (Hassaan et al., 2021b). The remnant topography was mimicking the pre-salt rift architecture and created preferential sediment deposition locations for the later prograded sediments in the Nordkapp Basin.

5.2.2 | Triassic sediment progradation: Depositional fairways and sediment routing patterns

Initiated during the earliest Triassic, the sedimentary wedges of the regionally developed Triassic delta system were sourced from the Urals in the southeast and prograded into the South Barents Sea Basin (Gilmullina et al., 2021) and farther westwards under regional subsidence conditions in the Norwegian Barents Sea (Eide et al., 2018; Glørstad-Clark et al., 2010; Klausen et al., 2015; Figures 5a and 17). The thickness of the earliest Triassic sequence S1 decreases to the WNW and SW distal parts, and gradually thins on the Bjarmeland and Finnmark platforms parallel to the strike of the Nordkapp Basin axis (Figure 5a). Furthermore, the updated regional thickness map of the earliest Triassic sequence S1 (including interpretation of all new available seismic) displays significant changes in contrast to the earlier similar map of Glørstad-Clark et al. (2010); this can be attributed to the internal variation of clinothems within the deltaic system (Figure 5a). We suggest that in the earliest Triassic the dominant sediment influx direction into the Nordkapp Basin was from the east to the west (Figures 5a and 6a) instead of southeast to northwest as proposed earlier (Glørstad-Clark et al., 2010; Grimstad, 2016; Rojo et al., 2019).

Hence, the prograding and quickly accumulating sequence S1 entered the Nordkapp Basin within the NENB segment first from the east (Figures 5a and 6a; Table 5). Several studies have recently proposed the Triassic progradational loading as the triggering mechanism of salt mobilisation to explain the observed post-salt geometries and structural style in the NENB segment (Figure 7; Grimstad, 2016; Rojo et al., 2019; Rowan & Lindsø, 2017). We support this and offer additional details in this context. The sediment accumulation was influenced by the syn-kinematic salt mobilisation due to the differential loading imposed by the prograding sediments of sequence S1 within the basin (Figures 6a, 7, and 14A2–A8). It seems that the salt structures were nucleated above the intra-basinal highs, whereas the minor mid-late Permian normal faulting was amplified by the accelerated sediment accumulation and loading of sequence S1.

The intense salt mobilisation strongly influenced the formation of depositional fairways and sediment routing patterns along the basin axis within the Nordkapp Basin. However, the formation of the initial depositional fairways also depends on the sediment influx direction over a highly complex base-salt rift architecture filled with LES (Figures 3, 4a, and 5A1). The progressive salt expulsion caused by the loading of prograding sediments formed the prominent NNW migrating depocenters and
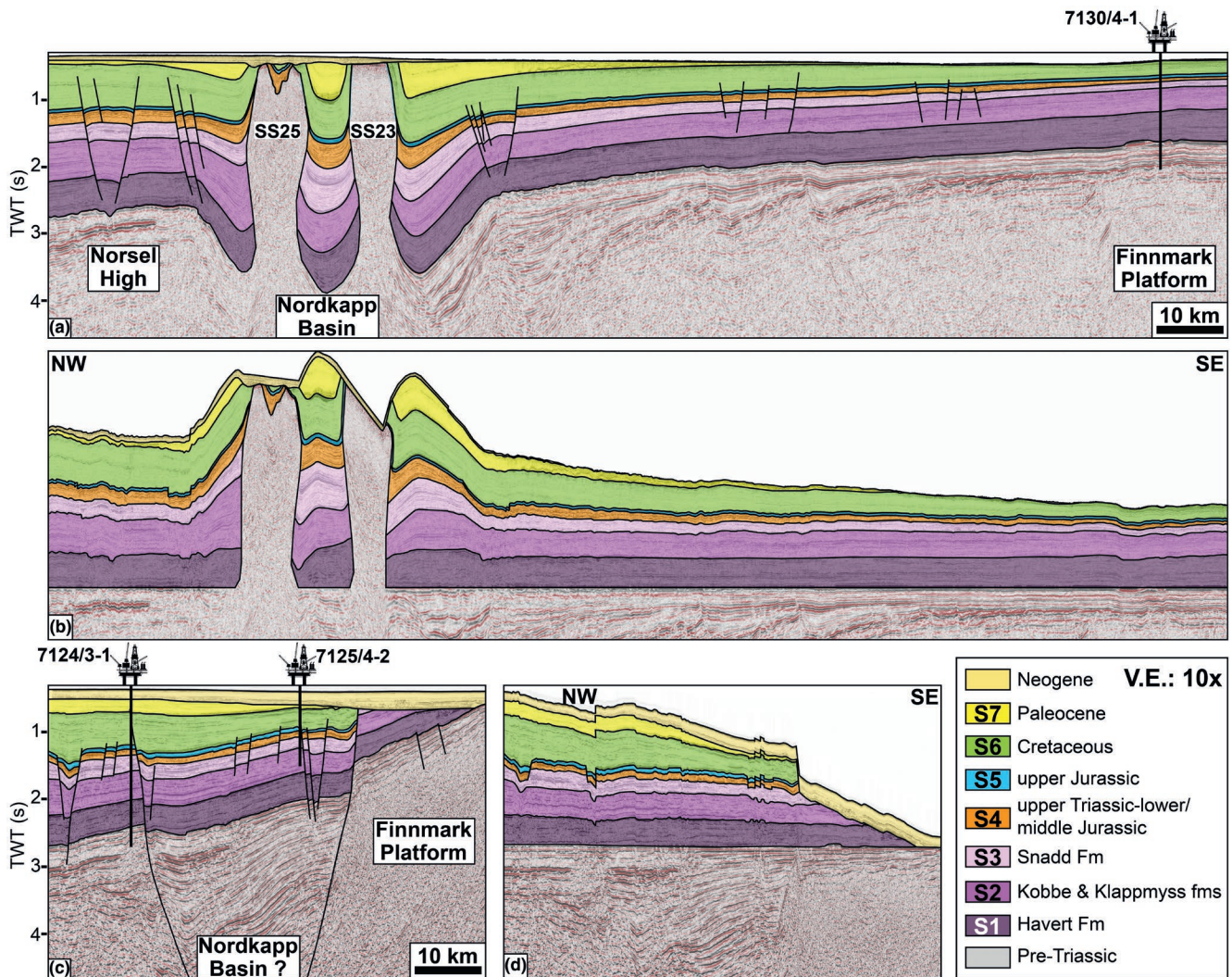
FIGURE 17 (a–b) Interpreted un-flattened and flattened seismic sections illustrating post-Permian sedimentary strata influenced by the salt structures (SS23 and SS25) in the southwestern (SWNB) Nordkapp Basin segment. (c–d) Interpreted un-flattened and flattened seismic sections outside of the Nordkapp Basin to the farther southwest shows no impact of the fault activity in the Triassic strata. It is noteworthy that in the Triassic the prograded sediments from the east were deposited under regional post-rift conditions in the Barents Sea (Eide et al., 2018; Glørstad-Clark et al., 2010; Klausen et al., 2015). TWT, two-way travel time, s; vertical exaggeration: 10×. Location of the sections as in Figure 1b

expulsion-rollover structures along with the turtle structure (Figure 7; Ge et al., 1997). The internal growth geometries are minimised towards SW following the bend of the SS1 salt wall where differential salt flow along the strike of the salt structure played an important role and caused differential mini-basin sink development (Figures 3c, 7b,c, 8a, and 14A2–A8). We suggest that the strike of precursor structural highs or master faults was as crucial as the velocity and direction of the prograding deltaic system for the complex salt structures formation. The rapid salt mobilisation created significant local topography and gave rise to the formation of mini-basins around the growing salt structures. The resulting basin topography strongly influenced the Triassic progradational fairways and dictated both where the initial deposition

could occur and the formation of distinct sediment routing patterns (Figure 5A1-2,B1-2). The depositional fairways and sediment routing patterns were primarily formed by differential loading and density-driven subsidence caused by the progradational sedimentation and have reduced the subsidence in the mini-basins that fall outside them (Figure 14A3–A6; Fernandez et al., 2020). Eventually, within the southwestern part of the CNB and the SWNB segments, the strata became isopachous similar to the Finnmark and Bjarmeland platforms due to less sediment input and thus insignificant salt mobilisation. We, therefore, suggest that the maximum sediment progradation and gravitational loading caused the most pronounced salt mobilisation to occur in the NENB segment, whereas these effects are more modest towards the SWNB

segment. Similarly, the salt was depleted from the LES diachronically along the strike of the Nordkapp Basin as the earliest passive diapirism occurred in the NENB segment due to the sediment influx direction, and then progressed to the CNB and SWNB segments (Figure 5a). We conclude that all the above processes led to a deformation outcome that outplayed the effect of the mid-late Permian extension in the Nordkapp Basin (Figures 5a, 6a, 14A2–A8, and 16A2–B2).

Continued salt mobilisation and passive diapirism significantly influenced the accumulation of the lower-middle Triassic sediments (sequence S2) and outpaced the effects of the prograding delta (Figures 5b and 6b; Table 5). The sediment input and loading direction had shifted from the east to the NW and had caused the formation of mini-basins to the northwest and intense salt evacuation to the south together with the rotation of the mini-basins where base-salt relief also facilitated the differential salt flow (Figures 13A3–B3, 14A9–A11, and 15A3–B3). The mini-basin rotation also depends on the progradational sedimentation direction and contraction (Figures 8b,c and 9b) (Callot et al., 2016; Duffy et al., 2021; Fernandez et al., 2020). The salt depletion and sediment accumulation were now mainly focused in the CNB segment, and were gradually minimised within the NENB and SWNB segments (Figure 6b; Table 5). Differential loading and NNW salt expulsion supported by the sediment progradation created NW migrating patterns and gave rise to the laterally most extensive depocenter in the NENB segment (Figures 7a, 10c, and 14A9–A11). As most of the salt was already evacuated from the LES, where the initial sediment routing patterns were located, these regions turned now into sediment by-pass areas where salt started to evacuate around them until the salt system had reached an equilibrium state, for example, the northern mini-basin of the SS1 salt wall (Figure 14A9–A11). Therefore, the preferred deposition locations for the thick prograding sequence S2 were mini-basins that were positioned adjacent to the initial depositional fairways and areas with thinner successions belonging to the S1 sequence (Figure 5A1–B1). Most of the salt beneath the NENB and CNB segments was evacuated by the end of sequence S2, probably due to the prominent differential loading and consequent intense salt expulsion. It is noteworthy that the sediment input direction was similar for the CNB and SWNB segments during the early-mid Triassic, but the salt evacuation and sediment accumulation were faster in the CNB segment (Figures 5b and 6). The restored LES thickness (mobile and non-mobile) along with seismic facies analysis suggest that the relative greater presence of non-mobile to mobile lithologies in the LES of the SWNB segment played an important role (Figures 11, 12, 15A1–B1, and 16A1–B1) and caused relatively slow passive

diapirism in the SWNB segment in contrast to the CNB segment (Figure 5B1–B2).

In the late Triassic (sequence S3), the sediment accumulation and consequent salt mobilisation were primarily focused in the SWNB segment as most of the salt from the LES was evacuated in the CNB and NENB segments by the end of the sequence S2 deposition (Figures 5c1-2 and 6c; Table 5) (Rojo et al., 2019). In the NENB segment, the NNW migrating depocenters moved to the southeastern edge of the salt-cored 'Veslekari Dome' anticline that formed due to progressive salt expulsion (Figures 5c, 7a, and 13A4). Passive diapirism continued as it is evident from the strata onlapping the salt structures forming CHS (i.e. tabular vs. tapered) and the downbuilding of mini-basins within the Nordkapp Basin (Figures 7, 11C1, 13B4, and 16A4–B4) (sensu Giles & Rowan, 2012; Pichel & Jackson, 2020). However, the along-strike growth development of few salt structures, that is, SS1 salt wall, was complicated during sediment deposition due to the amount of available mobile salt that was also influenced by the earlier intense salt depletion from the LES (Figures 7, 8b and 9b–d).

5.3 | Rejuvenation of salt structures: Influence of far-field stresses

5.3.1 | First rejuvenation phase: Triassic–Jurassic transition

During the late Triassic–mid Jurassic, most of the salt was already depleted from the LES in the NENB and CNB segments and the salt structures were covered by the thin sedimentary successions of sequence S4 (Figures 13A5–B5 and 14A5–B5,A13). However at the Triassic–Jurassic transition, the salt structures were rejuvenated and the salt-cored Veslekari Dome was formed due to reactivation of the deep Carboniferous structures caused by the propagated far-field stresses from the Novaya Zemlya fold-and-thrust belt (Figure 9b–d) (Faleide et al., 2018; Hassaan et al., 2020, 2021b; Indrevær et al., 2018; Müller et al., 2019). The SWNB segment had retained large amounts of salt in the LES, and this has facilitated the continued passive growth of the salt structures with acceleration due to the effect of the far-field shortening (Figures 5d1–2, 11, 12 and 16A5–B5). We suggest that the slight contractional rejuvenation of the salt structures has influenced the salt–sediment interactions, the type of evolved CHS, and the rotation of mini-basins in the Nordkapp Basin (Figures 11c1 and 15A5–B5; Callot et al., 2016; Giles & Rowan, 2012). The rejuvenation could also affect the style and routing of sediment dispersal systems in the mini-basins, as the along-strike growth of the salt structures is heterogeneous, and this could have influenced the distribution of the

upper Triassic–lower Jurassic reservoirs (within sequence S4) in the Nordkapp Basin.

A transition from tabular to tapered CHS are expected to occur for the upper Triassic and lower Jurassic strata in the NENB and CNB segments because the sediment accumulation rate outpaced the relative rate of salt structure growth when most of the salt has been evacuated (Figures 8a and 9b). However, the CHS-type also depends on the individual salt structural development, the sediment influx direction, the mini-basin rotation, and the rejuvenation intensity as some faults could be more reactivated in contrast to others (Hassaan et al., 2021a; Pichel & Jackson, 2020). In the SWNB segment, the rejuvenation became accelerated in cases with enhanced relative rate of salt structure growth in comparison with the sediment accumulation in the mini-basins and formed tabular CHS along the flanks of the salt structures (Figure 11b,c; Giles & Rowan, 2012; Rojo & Escalona, 2018). Deposition at or near the axial traces of drape folds within the CHS occur in salt-influenced rift basins, so that potential reservoir sandstones become deposited in channels and lobes that will pinch out up-dip. In this context, the transition from tabular to tapered or tabular dominated CHS would have significant implications for the distribution of the upper Triassic-lower Jurassic reservoirs (within sequence S4) in the mini-basins and for the development of stratigraphic traps at the diapir flanks (Figure 11b,c; Giles & Rowan, 2012; Hassaan et al., 2021a; Hearon et al., 2014; Pichel & Jackson, 2020). Therefore, the tabular CHS may have reservoir facies that are in direct contact with the diapir or that pinch-out less than 200 m away from it (Figure 11b,c) in contrast to the tapered CHS, which may contain reservoirs that pinch-out 300–1,000 m away from the diapir (Figure 9d; Pichel & Jackson, 2020).

At the same time, the reactivation of the Carboniferous structures, that is, faults and structural highs, and the rotation of the mini-basins have also facilitated the formation of the dwarf secondary mini-basins over the crest of the salt structures, that is, the DFa and DFd segments (Figures 9d and 10a). We suggest two possible scenarios for the formation of dwarf secondary mini-basins in the Nordkapp Basin at the Triassic–Jurassic transition: (1) fault reactivation that transferred the stress towards one side or flank of the salt structure and slightly rejuvenated it in contrast to the static side or flank, in this way facilitating extension at the centre of the feeder and creating a sag basin over the crest of the salt structure (Figure 9d2) or (2) due to far-field stresses few salt structures have been rejuvenated preferentially more than others and this created rotation of the mini-basins, whereas the precursor early-mid Triassic mini-basin rotation was caused by the sediment progradation. The mini-basin rotations in opposite direction may create extension at the axis of the feeder

and form dwarf secondary mini-basins over the crest of salt structures (Figure 15B5). In addition, the mobile salt from the source LES was almost exhausted that facilitated the dwarf secondary mini-basins development over the precursor diapirs. We suggest that these composite processes along with the formation of the tabular to tapered CHS, the salt wings and the megaflaps have all created a heterogeneous sedimentary environment for the deposition of the upper Triassic–lower Jurassic reservoirs in the Nordkapp Basin (Figures 9d and 11b–c).

A continued growth of the salt structures took place in the late Jurassic-early Cretaceous during the regional extension that affected the marginal fault complexes in the Nordkapp Basin and facilitated additional accommodation space (Figures 13A6–B6, 14A14, 15A6–B6 and 16A6–B6). During this time, the moderate growth of the salt structures can be attributed to gravity gliding and local salt evacuation (Nilsen et al., 1995; Rojo et al., 2019). Eventually, the entire Nordkapp Basin became covered by the prograding lower Cretaceous shelf-platform complex (Midtkandal et al., 2020) and the subsequent Paleocene sediments during a tectonically and halokinetically quiescent period (Figures 13A6–B6, 14A14, 15A6–B6 and 16A6–B6). However, the large thickness differences for the lower Cretaceous to Paleocene strata in the mini-basins compared with the same strata over the crest of the salt structures could be related to differential compaction and comparable with tertiary peripheral sinks developed around former highs above the salt structures (Jackson & Hudec, 2017; Trusheim, 1960). This is because the salt structures consist of non-compacted lithologies, whereas the siliciclastics in the mini-basins are prone to compaction below the overburden succession. Sediment loading and differential compaction have created additional accommodation space in the mini-basins that gives an impression of salt mobilisation due to large thickness variations (Figures 13B6, 14A14, 15A6–B6 and 16A6–B6).

5.3.2 | Second rejuvenation phase: Eocene

Another main phase of rejuvenation occurred likely during the early-mid Eocene, when reactivation of Carboniferous structures took place in response to far-field stresses from the transpressional Eurekan/Spitsbergen orogeny farther to the NW, and the strata that buried the salt structures were upturned along their flanks (Figures 13A7–B7, 14A15, 15A7–B7 and 16A7–B7; Gac et al., 2020; Hassaan et al., 2020, 2021a). In the Nordkapp Basin, the far-field stresses inverted some of the pre-salt normal faults along with reactivation of the structural highs depending on their orientation and controlled the style of salt reactivation (Figures 13A7–B7, 14A15, 15A7–B7 and 16A7–B7).

However, the rejuvenation intensity of the salt structures is partially dependent on the far-field stress propagation direction against the base-salt rift architecture but mainly to the salt structures type (walls vs. stocks), dip of the diapir flanks and distance of the salt structures with respect to the deformation front (Duffy et al., 2018; Hassanpour et al., 2021a, 2021b; Santolaria et al., 2021; Figures 3, 8b, and 9d1). It is worth noting that within sub-basin SB2 this reactivation turned the pre-salt normal fault into a reverse fault. The latter reached to the seafloor along with movement of the fault-block that raised the southern side of the mini-basin, squeezed the narrow salt structure and formed a secondary weld (Figures 8b and 13B6–7). We suggest that this specific reverse-fault could be related to the NTZ, which separates the NENB and CNB Nordkapp Basin segments (Figure 3b; Hassaan et al., 2021b).

The rejuvenation led to slight rotation of the mini-basins and made the potential near-diapir stratigraphic traps to become steeper and the late Triassic–mid Jurassic reservoirs (within sequence S4) at the centre of the mini-basins to become more tilted (Figures 13A7–B7, 14A15, 15A7–B7 and 16A7–B7). The steeper and tilted units are likely to develop over-pressure due to the upward rotation of strata, creating a large pressure head with top seal rocks that are unable to hold back a significant hydrocarbon column (Cumberpatch et al., 2021; Giles & Rowan, 2012; Heidari et al., 2019). Finally, the Cenozoic shelf uplift eroded post-middle Triassic to Eocene successions depending on the individual salt structure dynamics and increased the risk of leakage of significant volumes of hydrocarbons for possible earlier traps in the Nordkapp Basin (Figures 13A8–B8, 14A16, 15A8–B8 and 16A8–B8; Baig et al., 2016; Grimstad, 2016; Rojo et al., 2019).

6 | CONCLUSIONS

We used a large data set comprising regional 2D seismic reflection profiles, 3D seismic data, and available wells (exploration and shallow boreholes), in conjunction with 2D structural restoration and 1D backstripping to study the post-salt evolution of the Nordkapp Basin in the Barents Sea. The composite Nordkapp Basin evolved above a complex Carboniferous pre-salt rift architecture that resulted from the interaction of earlier (Timanian and Caledonian) basement structures and two extension phases and has affected the thickness and depositional facies of a laterally varying LES.

Initially, regional mid-late Permian extension influenced more the Caledonian than the Timanian structures beneath the Nordkapp Basin and reactivated pre-salt Carboniferous faults, leading to minor normal faulting in the lower-upper Permian strata and slight salt mobilisation towards the structural highs. The main salt mobilisation in the Nordkapp Basin took place in the earliest Triassic during sediment transport from the east, rapid sedimentation and differential loading. The intense salt depletion influenced the initial sediment transport and this caused sediment routings along the basin axis, which reduced the subsidence in the surrounding mini-basins. We suggest that the input direction, velocity and thickness of the approaching prograding sediments triggered and sustained the early to late passive diapirism, salt expulsion and the depletion of mobile salt from the ponds filled with the LES. However, the effect of the base-salt relief was also important as the smooth base-salt surface promoted a salt expulsion rollover structures accurately in the northeastern segment. However, the complex and dynamic base-salt relief dominated in the central segment of the Nordkapp Basin. In the early-mid Triassic, the input of prograding sediments and the regional thickness direction have changed towards the NW, facilitating progressive salt expulsion, shift in salt evacuation towards the south and rotation of mini-basins. By the end of the mid Triassic, most of the salt from the LES was depleted in the northeastern and central segments. In the late Triassic, passive diapirism focused on the southwestern segment, while some of the salt structures in the northeastern and central segments were covered by prograding sediments emphasizing, in this way, the along-strike salt structure development.

During the Triassic–Jurassic transition, minor rejuvenation of the salt structures took place due to reactivation of pre-salt Carboniferous structures caused by far-field stresses from the Novaya Zemlya fold-and-thrust belt to the east. We suggest that this minor rejuvenation caused further rotation of the developed mini-basins, formation of dwarf secondary mini-basins, and has influenced the sediment dispersal routings. Eventually, the prograding lower Cretaceous shelf-platform complex and subsequent Paleocene sediments buried the entire Nordkapp Basin during the tectonically and halokinetically quiescent period. A second phase of main rejuvenation of the salt structures likely took place in the early-mid Eocene due to far-field stresses from the transpressional Eurekan/Spitsbergen orogeny to the NW. The propagated stress potentially inverted pre-salt Carboniferous faults along with reactivation of the structural highs depending on their orientation. Finally, the Cenozoic shelf uplift caused the erosion of post-middle Triassic to Eocene successions in the Nordkapp Basin.

The current study highlights the significance of the interplay between sediment progradation, laterally varying LES, and the pre-salt rift architecture for the post-salt evolution in the Nordkapp Basin. The complex salt mobilisation and rejuvenation of the salt structures have influenced the

sediment dispersal in the mini-basins that may ultimately affect the distribution of potential reservoirs and source rocks within the Nordkapp Basin. The revealed processes and study outcomes can provide guidelines to understand other evaporite-dominated basins in the Barents Sea and salt-influenced rift basins in a worldwide perspective.

CONFLICT OF INTEREST

The authors declare that they have no conflict of interest.

AUTHOR CONTRIBUTIONS

M.H. and J.I.F designed and directed the research. M.H. interpreted the seismic data, and performed the 2D kinematic structural restoration and 1D backstripping. M.H., J.I.F., R.H.G., F.T and S.G. analysed the results. M.H. prepared the figures and wrote the manuscript text. All authors reviewed to the writing of the manuscript.

PEER REVIEW

The peer review history for this article is available at https://publons.com/publon/10.1111/bre.12602.

DATA AVAILABILITY STATEMENT

The data that support the findings of this study are available from NPD and TGS. Restrictions apply to the availability of these data, which were used under license for this study.

ORCID

Muhammad Hassaan https://orcid.org/0000-0001-6004-8557

REFERENCES

Baig, I., Faleide, J. I., Jahren, J., & Mondol, N. H. (2016). Cenozoic exhumation on the southwestern Barents Shelf: Estimates and uncertainties constrained from compaction and thermal maturity analyses. *Marine and Petroleum Geology*, *73*, 105–130. https://doi.org/10.1016/j.marpetgeo.2016.02.024

Barrère, C., Ebbing, J., & Gernigon, L. (2009). Offshore prolongation of Caledonian structures and basement characterisation in the western Barents Sea from geophysical modelling. *Tectonophysics*, *470*(1–2), 71–88. https://doi.org/10.1016/j.tecto.2008.07.012

Barrère, C., Ebbing, J., & Gernigon, L. (2011). 3-D density and magnetic crustal characterisation of the southwestern Barents Shelf: Implications for the offshore prolongation of the Norwegian Caledonides. *Geophysical Journal International*, *184*(3), 1147–1166.

Beauchamp, B. (1994). Permian climatic cooling in the Canadian Arctic. *Geological Society of America Special Paper*, *288*, 229–246.

Bjørlykke, K., Chuhan, F., Kjeldstad, A., Gundersen, E., Lauvrak, O., & Høeg, K. (2004). Modelling of sediment compaction during burial in sedimentary basins. In O. Stephansson, J. Hudson, & L. King (Eds.), *Coupled thermo-hydro-mechanical-chemical processes in geo-systems* (pp. 699–708). Elsevier.

Blaich, O. A., Tsikalas, F., & Faleide, J. I. (2017). New insights into the tectono-stratigraphic evolution of the southern Stappen High and its transition to Bjørnøya Basin, SW Barents Sea. *Marine and Petroleum Geology*, *85*, 89–105. https://doi.org/10.1016/j.marpetgeo.2017.04.015

Breivik, A. J., Gudlaugsson, S. T., & Faleide, J. I. (1995). Ottar Basin, SW Barents Sea: A major Upper Palaeozoic rift basin containing large volumes of deeply buried salt. *Basin Research*, *7*, 299–312. https://doi.org/10.1111/j.1365-2117.1995.tb00119.x

Bugge, T., Mangerud, G., Elvebakk, G., Mørk, A., Nilsson, I., Fanavoll, S., & Vigran, J. O. (1995). The Upper Palaeozoic succession on the Finnmark Platform, Barents Sea. *Norsk Geologisk Tidsskrift*, *75*(1), 3–30.

Callot, J.-P., Salel, J.-F., Letouzey, J., Daniel, J.-M., & Ringenbach, J.-C. (2016). Three-dimensional evolution of salt-controlled mini-basins: Interactions, folding, and megaflap development. *AAPG Bulletin*, *100*(9), 1419–1442. https://doi.org/10.1306/03101614087

Catuneanu, O., Galloway, W. E., Kendall, C. G. S. C., Miall, A. D., Posamentier, H. W., Strasser, A., & Tucker, M. E. (2011). Sequence stratigraphy: Methodology and nomenclature. *Newsletters on Stratigraphy*, *44*(3), 173–245. https://doi.org/10.1127/0078-0421/2011/0011

Clark, J., Stewart, S., & Cartwright, J. (1998). Evolution of the NW margin of the North Permian Basin, UK North Sea. *Journal of the Geological Society*, *155*(4), 663–676. https://doi.org/10.1144/gsjgs.155.4.0663

Clark, S., Glorstad-Clark, E., Faleide, J., Schmid, D., Hartz, E., & Fjeldskaar, W. (2014). Southwest Barents Sea rift basin evolution: Comparing results from backstripping and timeforward modelling. *Basin Research*, *26*(4), 550–566. https://doi.org/10.1111/bre.12039

Cumberpatch, Z., Finch, E., Kane, I., Pichel, L. M., Jackson, C., Kilhams, B., Hodgson, D., & Huuse, M. (2021). Halokinetic modulation of sedimentary thickness and architecture: A

numerical modelling approach. *Basin Reseach*. https://doi.org/10.1111/bre.12569

Dengo, C., & Røssland, K. (1992). Extensional tectonic history of the western Barents Sea. In R. M. Larsen, R. T. Larsen, H. Brekke & E. Talleraas (Eds.), *Structural and tectonic modelling and its application to petroleum geology* (pp. 91–107). Elsevier.

Duffy, O. B., Dooley, T. P., Hudec, M. R., Fernandez, N., Jackson, C. A. L., & Soto, J. I. (2021). Principles of shortening in salt basins containing isolated minibasins. *Basin Research*, *33*(3), 2089–2117. https://doi.org/10.1111/bre.12550

Duffy, O. B., Dooley, T. P., Hudec, M. R., Jackson, M. P., Fernandez, N., Jackson, C. A., & Soto, J. I. (2018). Structural evolution of salt-influenced fold-and-thrust belts: A synthesis and new insights from basins containing isolated salt diapirs. *Journal of Structural Geology*, *114*, 206–221. https://doi.org/10.1016/j.jsg.2018.06.024

Eide, C. H., Klausen, T. G., Katkov, D., Suslova, A. A., & Helland-Hansen, W. (2018). Linking an Early Triassic delta to antecedent topography: Source-to-sink study of the southwestern Barents Sea margin. *GSA Bulletin*, *130*(1–2), 263–283. https://doi.org/10.1130/B31639.1

Faleide, J. I., Gudlaugsson, S. T., & Jacquart, G. (1984). Evolution of the western Barents Sea. *Marine and Petroleum Geology*, *1*(2), 123–150. https://doi.org/10.1016/0264-8172(84)90082-5

Faleide, J. I., Pease, V., Curtis, M., Klitzke, P., Minakov, A., Scheck-Wenderoth, M., Kostyuchenko, S., & Zayonchek, A. (2018). Tectonic implications of the lithospheric structure across the Barents and Kara shelves. *Geological Society, London, Special Publications*, *460*(1), 285–314. https://doi.org/10.1144/SP460.18

Faleide, J. I., Tsikalas, F., Breivik, A. J., Mjelde, R., Ritzmann, O., Engen, Ø., Wilson, J., & Eldholm, O. (2008). Structure and evolution of the continental margin off Norway and the Barents Sea. *Episodes*, *31*(1), 82–91. https://doi.org/10.18814/epiiugs/2008/v31i1/012

Faleide, J. I., Vågnes, E., & Gudlaugsson, S. T. (1993). Late Mesozoic-Cenozoic evolution of the south-western Barents Sea in a regional rift-shear tectonic setting. *Marine and Petroleum Geology*, *10*(3), 186–214. https://doi.org/10.1016/0264-8172(93)90104-Z

Fernandez, N., Hudec, M. R., Jackson, C.-A.-L., Dooley, T. P., & Duffy, O. B. (2020). The competition for salt and kinematic interactions between minibasins during density-driven subsidence: Observations from numerical models. *Petroleum Geoscience*, *26*(1), 3–15. https://doi.org/10.1144/petgeo2019-051

Gabrielsen, R. (1984). Long-lived fault zones and their influence on the tectonic development of the southwestern Barents Sea. *Journal of the Geological Society*, *141*(4), 651–662. https://doi.org/10.1144/gsjgs.141.4.0651

Gabrielsen, R. H., Faerseth, R. B., & Jensen, L. N. (1990). *Structural elements of the Norwegian Continental Shelf. Pt. 1. The Barents Sea Region*. Norwegian Petroleum Directorate.

Gabrielsen, R. H., Grunnaleite, I., & Rasmussen, E. (1997). Cretaceous and tertiary inversion in the Bjørnøyrenna Fault Complex, south-western Barents Sea. *Marine and Petroleum Geology*, *14*, 165–178. https://doi.org/10.1016/S0264-8172(96)00064-5

Gabrielsen, R., Kløvjan, O., Rasmussen, A., & Stølan, T. (1992). Interaction between halokinesis and faulting: Structuring of the margins of the Nordkapp Basin, Barents Sea region. *Proceedings Structural and Tectonic Modelling and Its Implication to Petroleum Geology; Proceedings1992*, *1*, 121–131.

Gac, S., Minakov, A., Shephard, G. E., Faleide, J. I., & Planke, S. (2020). Deformation analysis in the Barents Sea in relation to Paleogene transpression along the Greenland-Eurasia plate boundary. *Tectonics*, *39*. https://doi.org/10.1029/2020TC006172

Ge, H., Jackson, M. P., & Vendeville, B. C. (1997). Kinematics and dynamics of salt tectonics driven by progradation. *AAPG Bulletin*, *81*(3), 398–423.

Gee, D., Bogolepova, O., & Lorenz, H. (2006). The Timanide, Caledonide and Uralide orogens in the Eurasian high Arctic, and relationships to the palaeo-continents Laurentia, Baltica and Siberia. *Geological Society, London, Memoirs*, *32*(1), 507–520.

Gernigon, L., & Brönner, M. (2012). Late Palaeozoic architecture and evolution of the southwestern Barents Sea: Insights from a new generation of aeromagnetic data. *Journal of the Geological Society*, *169*(4), 449–459. https://doi.org/10.1144/0016-76492011-131

Gernigon, L., Brönner, M., Dumais, M.-A., Gradmann, S., Grønlie, A., Nasuti, A., & Roberts, D. (2018). Basement inheritance and salt structures in the SE Barents Sea: Insights from new potential field data. *Journal of Geodynamics*, *119*, 82–106. https://doi.org/10.1016/j.jog.2018.03.008

Gernigon, L., Brönner, M., Roberts, D., Olesen, O., Nasuti, A., & Yamasaki, T. (2014). Crustal and basin evolution of the southwestern Barents Sea: From Caledonian orogeny to continental breakup. *Tectonics*, *33*(4), 347–373.

Giles, K. A., & Rowan, M. G. (2012). Concepts in halokinetic-sequence deformation and stratigraphy. *Geological Society, London, Special Publications*, *363*(1), 7–31. https://doi.org/10.1144/SP363.2

Gilmullina, A., Klausen, T. G., Paterson, N. W., Suslova, A., & Eide, C. H. (2021). Regional correlation and seismic stratigraphy of Triassic Strata in the Greater Barents Sea: Implications for sediment transport in Arctic basins. *Basin Research*, *33*(2), 1546–1579. https://doi.org/10.1111/bre.12526

Glørstad-Clark, E., Faleide, J. I., Lundschien, B. A., & Nystuen, J. P. (2010). Triassic seismic sequence stratigraphy and paleogeography of the western Barents Sea area. *Marine and Petroleum Geology*, *27*(7), 1448–1475. https://doi.org/10.1016/j.marpetgeo.2010.02.008

Gradstein, F. M., & Ogg, J. G. (2020). The chronostratigraphic scale. In F. M. Gradstein, J. G. Ogg, M. D. Schmitz & G. M. Ogg (Eds.), *Geologic Time Scale 2020* (pp. 21–32). Elsevier.

Grimstad, S. (2016). *Salt tectonics in the central and northeastern Nordkapp Basin, Barents Sea* (Master thesis) (pp. 1–127). University of Oslo.

Gudlaugsson, S., Faleide, J., Johansen, S., & Breivik, A. (1998). Late Palaeozoic structural development of the south-western Barents Sea. *Marine and Petroleum Geology*, *15*(1), 73–102. https://doi.org/10.1016/S0264-8172(97)00048-2

Hassaan, M., Faleide, J. I., Gabrielsen, R. H., & Tsikalas, F. (2020). Carboniferous graben structures, evaporite accumulations and tectonic inversion in the southeastern Norwegian Barents Sea. *Marine and Petroleum Geology*, *112*, 104038. https://doi.org/10.1016/j.marpetgeo.2019.104038

Hassaan, M., Faleide, J. I., Gabrielsen, R. H., & Tsikalas, F. (2021a). Architecture of the evaporite accumulation and salt structures dynamics in Tiddlybanken Basin, southeastern Norwegian Barents Sea. *Basin Research*, *33*(1), 91–117. https://doi.org/10.1111/bre.12456

Hassaan, M., Faleide, J. I., Gabrielsen, R. H. & Tsikalas, F. (2021b). The effects of Carboniferous basin configuration and structural

inheritance on evaporite distribution and the development of salt structures in the Nordkapp Basin, Barents Sea–Part I. https://doi.org/10.1111/bre.12565

Hassanpour, J., Yassaghi, A., Muñoz, J. A., & Jahani, S. (2021a). Salt tectonics in a double salt-source layer setting (Eastern Persian Gulf, Iran): Insights from interpretation of seismic profiles and sequential cross-section restoration. *Basin Research*, *33*(1), 159–185. https://doi.org/10.1111/bre.12459

Hassanpour, J., Muñoz, J. A., Yassaghi, A., Ferrer, O., Jahani, S., Santolaria, P., & SeyedAli, S. M. (2021b). Impact of salt layers interaction on the salt flow kinematics and diapirism in the Eastern Persian Gulf, Iran: Constraints from seismic interpretation, sequential restoration, and physical modelling. *Tectonophysics*, *811*, 228887.

Hearon, T. E., IV, Rowan, M. G., Giles, K. A., & Hart, W. H. (2014). Halokinetic deformation adjacent to the deepwater Auger diapir, Garden Banks 470, northern Gulf of Mexico: Testing the applicability of an outcrop-based model using subsurface data. *Interpretation*, *2*(4), SM57–SM76. https://doi.org/10.1190/INT-2014-0053.1

Heidari, M., Nikolinakou, M. A., Hudec, M. R., & Flemings, P. B. (2019). Influence of a reservoir bed on diapirism and drilling hazards near a salt diapir: A geomechanical approach. *Petroleum Geoscience*, *25*(3), 282–297. https://doi.org/10.1144/petgeo2018-113

Henriksen, E., Bjørnseth, H., Hals, T., Heide, T., Kiryukhina, T., Kløvjan, O., Larssen, G. B., Ryseth, A. E., Rønning, K., Sollid, K., & Stoupakova, A. (2011). Uplift and erosion of the greater Barents Sea: Impact on prospectivity and petroleum systems. *Geological Society, London, Memoirs*, *35*(1), 271–281.

Indrevær, K., Gac, S., Gabrielsen, R. H., & Faleide, J. I. (2018). Crustal-scale subsidence and uplift caused by metamorphic phase changes in the lower crust: A model for the evolution of the Loppa High area, SW Barents Sea from late Paleozoic to Present. *Journal of the Geological Society*, *175*(3), 497–508. https://doi.org/10.1144/jgs2017-063

Jackson, C. A. L., Duffy, O. B., Fernandez, N., Dooley, T. P., Hudec, M. R., Jackson, M. P., & Burg, G. (2020). The stratigraphic record of minibasin subsidence, Precaspian Basin, Kazakhstan. *Basin Research*, *32*(4), 739–763. https://doi.org/10.1111/bre.12393

Jackson, C. A. L., Elliott, G. M., Royce-Rogers, E., Gawthorpe, R. L., & Aas, T. E. (2018). Salt thickness and composition influence rift structural style, northern North Sea, offshore Norway. *Basin Research*, *31*(3), 514–538.

Jackson, M. P., & Hudec, M. R. (2017). *Salt tectonics: Principles and practice*. Cambridge University Press.

Jensen, L., & Sørensen, K. (1992). Tectonic framework and halokinesis of the Nordkapp Basin, Barents Sea. In R. M. Larsen, R. T. Larsen, H. Brekke & E. Talleraas (Eds.), *Structural and tectonic modelling and its application to petroleum geology* (pp. 109–120). Elsevier.

Klausen, T. G., Ryseth, A. E., Helland-Hansen, W., Gawthorpe, R., & Laursen, I. (2015). Regional development and sequence stratigraphy of the Middle to Late Triassic Snadd formation, Norwegian Barents Sea. *Marine and Petroleum Geology*, *62*, 102–122. https://doi.org/10.1016/j.marpetgeo.2015.02.004

Koyi, H., Talbot, C. J., & Tørudbakken, B. O. (1993). Salt diapirs of the southwest Nordkapp Basin: Analogue modelling. *Tectonophysics*, *228*(3–4), 167–187. https://doi.org/10.1016/0040-1951(93)90339-L

Koyi, H., Talbot, C. J., & Tørudbakken, B. O. (1995). Salt tectonics in the Northeastern Nordkapp basin, Southwestern Barents sea. *AAPG Memoir*, *65*, 437–447.

Larssen, G., Elvebakk, G., Henriksen, L. B., Kristensen, S., Nilsson, I., Samuelsberg, T. J., Svånå, T.A., Stemmerik, L., & Worsley, D. (2002). Upper Palaeozoic lithostratigraphy of the Southern Norwegian Barents Sea. *Norwegian Petroleum Directorate Bulletin*, *9*, 76.

Lasabuda, A., Laberg, J. S., Knutsen, S.-M., & Høgseth, G. (2018). Early to middle Cenozoic paleoenvironment and erosion estimates of the southwestern Barents Sea: Insights from a regional mass-balance approach. *Marine and Petroleum Geology*, *96*, 501–521. https://doi.org/10.1016/j.marpetgeo.2018.05.039

Lasabuda, A., Laberg, J. S., Knutsen, S.-M., & Safronova, P. (2018). Cenozoic tectonostratigraphy and pre-glacial erosion: A mass-balance study of the northwestern Barents Sea margin, Norwegian Arctic. *Journal of Geodynamics*, *119*, 149–166. https://doi.org/10.1016/j.jog.2018.03.004

Marello, L., Ebbing, J., & Gernigon, L. (2013). Basement inhomogeneities and crustal setting in the Barents Sea from a combined 3D gravity and magnetic model. *Geophysical Journal International*, *193*(2), 557–584. https://doi.org/10.1093/gji/ggt018

Mattingsdal, R., Høy, T., Simonstad, E., & Brekke, H. (2015). An updated map of structural elements in the southern Barents Sea. *Paper presented at the 31st Geological Winter Meeting*.

Midtkandal, I., Faleide, T. S., Faleide, J. I., Planke, S., Anell, I., & Nystuen, J. P. (2020). Nested intrashelf platform clinoforms—Evidence of shelf platform growth exemplified by Lower Cretaceous strata in the Barents Sea. *Basin Research*, *32*(2), 216–223.

Mondol, N. H., Bjørlykke, K., Jahren, J., & Høeg, K. (2007). Experimental mechanical compaction of clay mineral aggregates—Changes in physical properties of mudstones during burial. *Marine and Petroleum Geology*, *24*, 289–311. https://doi.org/10.1016/j.marpetgeo.2007.03.006

Müller, R., Klausen, T., Faleide, J., Olaussen, S., Eide, C., & Suslova, A. (2019). Linking regional unconformities in the Barents Sea to compression-induced forebulge uplift at the Triassic-Jurassic transition. *Tectonophysics*, *765*, 35–51. https://doi.org/10.1016/j.tecto.2019.04.006

Nilsen, K. T., Vendeville, B. C. & Johansen, J.-T. (1995). Influence of regional tectonics on halokinesis in the Nordkapp Basin, Barents Sea. In M. P. A. Jackson, D. G. Roberts & S. Snelson (Eds.), *Salt tectonics: a global perspective* Vol. 65, (pp. 413–436). AAPG Memoir.

Pease, V., Scarrow, J., Silva, I. N., & Cambeses, A. (2016). Devonian magmatism in the Timan Range, Arctic Russia—Subduction, post-orogenic extension, or rifting? *Tectonophysics*, *691*, 185–197.

Pichel, L. M., Finch, E., & Gawthorpe, R. L. (2019). The impact of pre-salt rift topography on salt tectonics: A discrete-element modeling approach. *Tectonics*, *38*(4), 1466–1488. https://doi.org/10.1029/2018TC005174

Pichel, L. M., & Jackson, C. A. L. (2020). Four-dimensional variability of composite Halokinetic sequences. *Basin Research*, *32*(6), 1277–1299. https://doi.org/10.1111/bre.12428

Rice, A., Gayer, R., Robinson, D., & Bevins, R. (1989). Strike-slip restoration of the Barents Sea Caledonides Terrane, Finnmark, north Norway. *Tectonics*, *8*(2), 247–264. https://doi.org/10.1029/TC008i002p00247

Ritzmann, O., & Faleide, J. I. (2007). Caledonian basement of the western Barents Sea. *Tectonics*, *26*(5), 1–20. https://doi.org/10.1029/2006TC002059

Roberts, D. (1972). *Tectonic deformation in the Barents Sea region of Varanger peninsula*. Universitetsforlaget.

Roberts, D., & Gee, D. G. (1985). An introduction to the structure of the Scandinavian Caledonides. *The Caledonide Orogen–scandinavia and Related Areas*, *1*, 55–68.

Rodriguez, C. R., Jackson, C. L., Rotevatn, A., Bell, R. E., & Francis, M. (2018). Dual tectonic-climatic controls on salt giant deposition in the Santos Basin, offshore Brazil. *Geosphere*, *14*(1), 215–242.

Rojo, L. A., Cardozo, N., Escalona, A., & Koyi, H. (2019). Structural style and evolution of the Nordkapp Basin, Norwegian Barents Sea. *AAPG Bulletin*, *103*, 2177–2217. https://doi.org/10.1306/01301918028

Rojo, L. A., & Escalona, A. (2018). Controls on minibasin infill in the Nordkapp Basin: Evidence of complex Triassic synsedimentary deposition influenced by salt tectonics. *AAPG Bulletin*, *102*(7), 1239–1272. https://doi.org/10.1306/0926171524316523

Rowan, M. G., & Ratliff, R. A. (2012). Cross-section restoration of salt-related deformation: Best practices and potential pitfalls. *Journal of Structural Geology*, *41*, 24–37.

Rowan, M. G., & Lindsø, S. (2017). Salt Tectonics of the Norwegian Barents Sea and Northeast Greenland Shelf. In J. I. Soto, J. F. Flinch & G. Tari (Eds.), *Permo-Triassic Salt Provinces of Europe, North Africa and the Atlantic Margins* (pp. 265–286). Elsevier.

Rowan, M. G., Urai, J. L., Fiduk, J. C., & Kukla, P. A. (2019). Deformation of intrasalt competent layers in different modes of salt tectonics. *Solid Earth*, *10*(3), 987–1013. https://doi.org/10.5194/se-10-987-2019

Santolaria, P., Ferrer, O., Rowan, M. G., Snidero, M., Carrera, N., Granado, P., Muñoz, J. A., Roca, E., Schneider, C. L., Piña, A., & Zamora, G. (2021). Influence of preexisting salt diapirs during thrust wedge evolution and secondary welding: Insights from analog modeling. *Journal of Structural Geology*, *149*, 104374. https://doi.org/10.1016/j.jsg.2021.104374

Schiffer, C., Doré, A. G., Foulger, G. R., Franke, D., Geoffroy, L., Gernigon, L., Holdsworth, B., Kusznir, N., Lundin, E., McCaffrey, K., Peace, A. L., Petersen, K. D., Phillips, T. B., Stephenson, R., Stoker, M. S., & Welford, J. K. (2020). Structural inheritance in the North Atlantic. *Earth-Science Reviews*, *206*, 102975. https://doi.org/10.1016/j.earscirev.2019.102975

Sclater, J. G., & Christie, P. A. F. (1980). Continental stretching: An explanation of the post-mid Cretaceous subsidence of the Central North Sea Basin. *Journal of Geophysical Research*, *85*, 3711–3739 [Appendix A, 3730–3735].

Stemmerik, L. (2000). Late Palaeozoic evolution of the North Atlantic margin of Pangea. *Palaeogeography, Palaeoclimatology, Palaeoecology*, *161*(1–2), 95–126. https://doi.org/10.1016/S0031-0182(00)00119-X

Stewart, S. (2007). Salt tectonics in the North Sea Basin: A structural style template for seismic interpreters. *Special Publication-Geological Society of London*, *272*, 361–396. https://doi.org/10.1144/GSL.SP.2007.272.01.19

Stewart, S., Ruffell, A., & Harvey, M. (1997). Relationship between basement-linked and gravity-driven fault systems in the UKCS salt basins. *Marine and Petroleum Geology*, *14*(5), 581–604. https://doi.org/10.1016/S0264-8172(97)00008-1

Trusheim, F. (1960). Mechanism of salt migration in northern Germany. *AAPG Bulletin*, *44*(9), 1519–1540.

Tsikalas, F., Blaich, O. A., Faleide, J. I., & Olaussen, S. (2021). Stappen High-Bjørnøya tectono-sedimentary element, Barents Sea. In S. S. Drachev, H. Brekke, E. Henriksen, & T. Moore (Eds.), *Sedimentary successions of the Arctic Region and their hydrocarbon prospectivity. Geological Society, London, Memoirs* (Vol. *57*). https://doi.org/10.1144/M57-2016-24

Tsikalas, F., Faleide, J. I., Eldholm, O., & Blaich, O. A. (2012). The NE Atlantic conjugate margins. In D. G. Roberts & A. W. Bally (Eds.), *Regional geology and tectonics: Phanerozoic passive margins, Cratonic Basins and Global Tectonic Maps* (pp. 141–200). Elsevier.

Warren, J. K. (2016). *Evaporites: A geological compendium*. Springer.

Withjack, M. O., & Callaway, S. (2000). Active normal faulting beneath a salt layer: An experimental study of deformation patterns in the cover sequence. *AAPG Bulletin*, *84*(5), 627–651.